Nitrogen Doped Titanium Dioxide (N-TiO$_2$): Synopsis of Synthesis Methodologies, Doping Mechanisms, Property Evaluation and Visible Light Photocatalytic Applications

Thillai Sivakumar Natarajan [1],*, Velusamy Mozhiarasi [2] and Rajesh J. Tayade [3],*

[1] Environmental Science Laboratory, CSIR-Central Leather Research Institute (CSIR-CLRI), Chennai 600020, Tamil Nadu, India

[2] CLRI Regional Centre Jalandhar, CSIR-Central Leather Research Institute (CSIR-CLRI), Jalandhar 144021, Punjab, India; mozhiarasi@clri.res.in

[3] CSIR-Central Salt and Marine Chemicals Research Institute (CSIR-CSMCRI), Bhavnagar 364002, Gujarat, India

* Correspondence: thillai@clri.res.in or tsknatarajan@gmail.com (T.S.N.); tayade@csmcri.res.in or rtayade@gmail.com (R.J.T.)

Abstract: Titanium dioxide (TiO$_2$) is one of the stable and potential metal oxide semiconductor nanomaterials with flexible properties which allows them to be used in a variety of applications (i.e., environmental remediation, energy storage and production, and also as a pigment in personal care products, etc.). However, its low surface area, poor adsorption capacity and high bandgap energy (~3.2 eV) prevents its full potency. Especially, TiO$_2$ with high bandgap (~3.2 eV) reduces its visible light absorption capacity and catalytic efficiency. Various modification processes (i.e., metal and non-metal doping, composite materials (mixed metal oxide, high surface area adsorbents), and dye sensitization etc.) have been accomplished for stimulating the characteristics of TiO$_2$ and the associated catalytic efficiency. Among the modifications, the non-metal doping process in TiO$_2$, specifically nitrogen doping, is one of the efficient dopants for enhancing the photocatalytic efficiency of TiO$_2$ in the presence of visible light irradiation. However, the morphology of TiO$_2$, structural changes in TiO$_2$ during N-doping, properties (e.g., morphology and electronic) of N-doped TiO$_2$ and also reaction operational parameters (e.g., doping concentration) hold a greater impact for enhancing the photocatalytic properties of TiO$_2$ either positively or negatively. Furthermore, the synthesis methodologies have a major influence on the synthesis of stable N-TiO$_2$ with pronounced photocatalytic efficiencies. Nevertheless, the methodologies for highly stable N-TiO$_2$ synthesis, properties evaluation and their correlation with photocatalytic efficiencies are still not appropriately stabilized to accomplish the commercial utilization of N-TiO$_2$. Therefore, this review article focuses on the synopsis of various synthesis methodologies and either their efficiencies or inefficiencies, the mechanism involved in the doping processes, changes in the structural, electronic and morphological properties observed due to the N-doping along with the photocatalytic capacity. Furthermore, the opportunities, challenges and future requirements linked to the development of durable N-doped TiO$_2$-based semiconductor nanomaterials for efficient catalytic performance is also represented.

Keywords: N-TiO$_2$; photocatalysis; visible light; pollutants degradation; water splitting

1. Introduction

Since the discovery of water splitting using TiO$_2$ by Fujishima and Honda [1], TiO$_2$ is a well-accepted stable and widely utilized metal-oxide-based semiconductor nanomaterial as photocatalyst for the decomposition of environmental pollutants (water, air and soil) and renewable energy (e.g., hydrogen) production. This could be ascribed to the unique features of TiO$_2$ materials such as low toxicity, chemical and biological stability, long durability, high photocatalytic activity, strength against photocorrosion, cost-effectiveness

and abundant availability. Furthermore, due to these unique characteristics of TiO_2, it has been widely used as a pigment in various products (i.e., toothpastes, paints, medicines, plastics, sunscreens and textiles, etc.) preparation. Furthermore, the high hydrophilicity of TiO_2 received significant industrial application, such as preparation of self-cleaning surfaces and antifogging mirrors, and it also possesses outstanding anticorrosion properties. In addition, TiO_2 could be supported on various solid materials which encourage its repeated usage [2–7]. Therefore, TiO_2 has been extensively used for various commercial/practical applications. Nevertheless, the practical application of TiO_2 materials in environmental pollutants degradation and renewable energy production is still limited. TiO_2 material could only be activated in the presence of ultraviolet (UV) light irradiation (high bandgap energy, ~3.2 eV) and could not be effectively used in solar light irradiation containing 2–3% UV light, 40–43% visible light and 50–55% near infrared light; as well as indoor room light (fluorescent, contains a small amount of UV light) irradiation. In addition, the low surface area and poor adsorption capacity of TiO_2 and high rate of recombination of photogenerated charge carriers on TiO_2 surface prevent its full potency in practical application [8–10].

In order for effective utilization of the solar spectrum by TiO_2, to decrease the recombination rate of photogenerated charge carriers and to enhance the associated photocatalytic property, the research on narrowing/lowering of the TiO_2 bandgap energy has been carried out by metal ion and non-metal ion doping, bi or tri-metal co-doping, surface sensitization, introduction of oxygen (O) defects and making composites (binary or tertiary) by coupling with other semiconductors and graphene-based materials, respectively [6,9,11–16]. In addition, the particle size of the TiO_2 is a crucial factor that influences its surface structure and properties resulting in the improved photocatalytic performance of the TiO_2. Similarly, the surface area and the adsorption capacity of TiO_2 is improved by coupling with high surface area adsorbent (carbon (activated carbon, biochar, nanotube), biochar, zeolite, silica and clays, etc.) materials and thus resulting in various catalytic performances [17–25].

Among the modifications, metal and non-metal doping is being considered as an efficient process by the introduction of new energy levels between the conduction and valence band of the TiO_2 leading to the efficient visible absorption of light, charge carriers separation and migration properties, and change in particle size and morphology of TiO_2 and other surface characteristics that improved the photocatalytic activities of TiO_2 catalysts. However, the additional high cost associated with the preparation of metal-doped TiO_2 lowers its full commercial potency. Some of the metal-doped TiO_2 have not been applied/used for real scale applications because they showed poor photocatalytic capacity and reproducibility. Therefore, the non-metal (N, S, P, B, C, F) doping on TiO_2 has been studied. Among these non-metals, it is observed that the nitrogen doping into TiO_2 (N-TiO_2), provides visible light responsive photocatalysts and received significant attention because of their comparable atomic size, low ionization energy, high electronegativity, stability and cost-effectiveness [13,26,27]. Further, the nitrogen doping improves the photogenerated charge carrier's separation and migration rates, which enhances the visible light photocatalytic efficiency. For the first time, Sato prepared NOx-doped TiO_2 and evaluated its catalytic activity by the oxidation of carbon monoxide and ethane and by oxygen isotope equilibration under the irradiation of visible light [28]. Later, Asahi et al. synthesized $TiO_{2-x}N_x$ thin films, proving that nitrogen doping is a substitutional one that showed higher photocatalytic ability than the undoped TiO_2 under the irradiation of visible light, however, it exhibited similar activity under UV light [29]. Subsequently, significant research has been carried out on the development of nitrogen-doped TiO_2 using various synthesis methodologies, studying the doping mechanism, characteristics and stability of the catalyst, and also providing evidences for improved visible light photocatalytic performance of N-TiO_2. Web of science bibliometrics analysis for the last 20 years (2001–2021) showed the increasing trend of research publication on N-TiO_2 (Figure 1). In the years from 2001 to 2010, the research communications on N-TiO_2 is 1106 which is significantly enhanced to 4109 in the years from 2011 to 2021. This shows the importance

of research on the development of N-TiO$_2$ materials. Despite the various studies available on N-TiO$_2$, the optimized synthesis methodologies, nitrogen doping mechanism, the stability and reusability of the materials are still unclear, and controversies regarding their commercial application also existed. Therefore, this review article describes the synthesis methodologies and mechanism of nitrogen doping, changes in the structural, morphological, electronic characteristics and photocatalytic performance of the N-doped TiO$_2$. This review also provides a comprehensive overview of enhancement in the catalytic reaction parameters (e.g., lifetime of the photoproduced charge carriers and reactive radical species) and the associated visible light photocatalytic application of N-doped TiO$_2$. Furthermore, future suggestions and prospects on the synthesis of highly durable nitrogen-doped TiO$_2$ and possibilities for their commercial usability are also summarized and discussed.
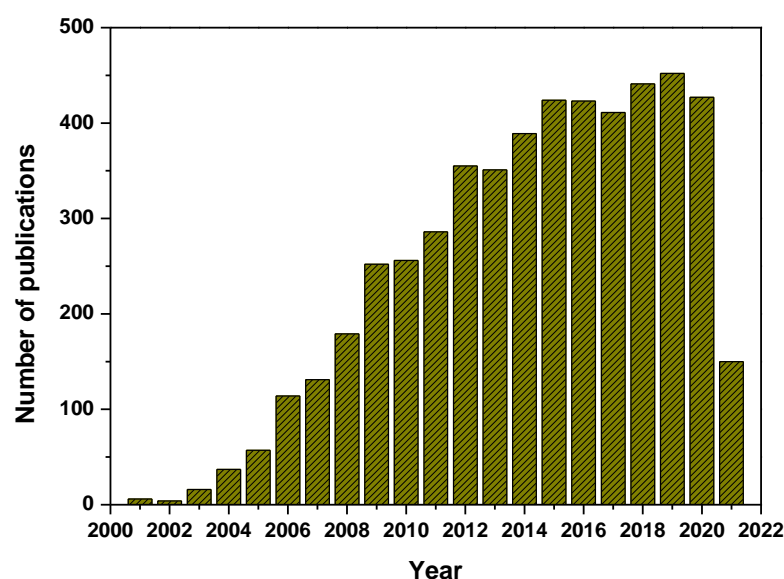

Figure 1. Number of publications on N-doped TiO$_2$ photocatalysts (source: Web of Science, keywords for searching: N-doped TiO$_2$, nitrogen-doped TiO$_2$, N-TiO$_2$ and TiO$_{2-x}$N$_x$).

2. Principles of TiO$_2$ Photocatalysis

Photocatalysis is one of the advanced oxidation processes, and involves production of electron-hole pairs upon irradiation of suitable light on the surface of semiconductor nanomaterials (e.g., TiO$_2$) followed by production of reactive radical species occurring for redox reactions with pollutants (Equations (1)–(11), Figure 2a). When the TiO$_2$ material is irradiated with light energy equal or greater than its bandgap energy, it excites the electrons (e$^-$) in the valence band (VB) to conduction band (CB), leaving behind holes (h$^+$) in the valence band (VB) of the semiconductor nanomaterial. Furthermore, these charge carriers react with the adsorbed water molecules or hydroxyl (−OH) groups on the nanomaterial's surface or dissolved oxygen in the reaction medium. Subsequently, it generates reactive radical species, such as superoxide radical anion (O$_2$$^{\bullet-}$) and hydroxyl ($^\bullet$OH) radicals, which degrade and mineralize the pollutants adsorbed on the nanomaterial's surface into water, carbon dioxide and other inorganic anions. In addition, the holes in the VB directly oxidize the pollutants adsorbed on the nanomaterial's surface. Furthermore, the electrons in the CB indirectly reduce the pollutants using hydroxyl ($^\bullet$OH) radicals formed during cleavage of in situ formed hydrogen peroxide (H$_2$O$_2$), which is formed by reaction between the superoxide radical anion (O$_2$$^-$) and proton (H$^+$) [30]. In the case of N-TiO$_2$, the isolated N 2p narrow band forms above the O 2p in the VB which is responsible for the visible light response of N-TiO$_2$ (Figure 2b). In addition, the recombination of photogenerated charge carriers might occur, which liberates heat that decreases the photocatalytic efficiency of

TiO$_2$. Therefore, the photogenerated charge carrier's generation, separation and transfer efficiency are the vital parameters for efficient photocatalytic activity.
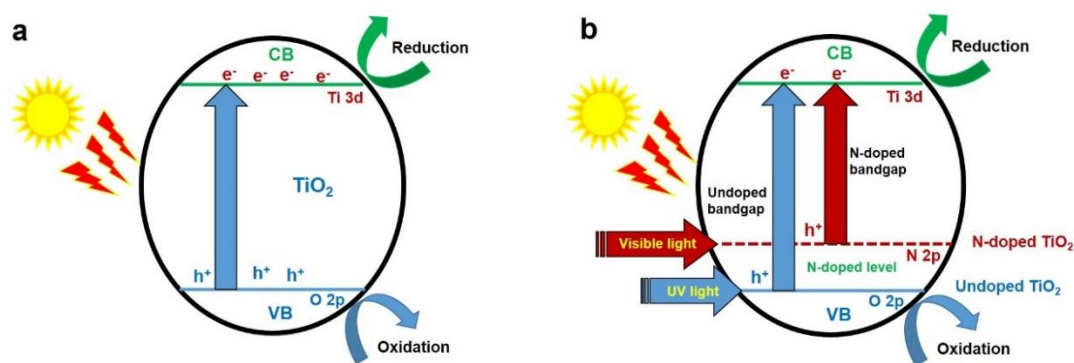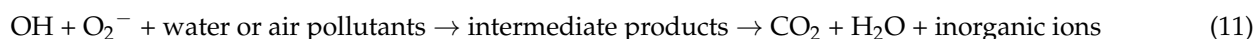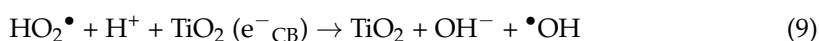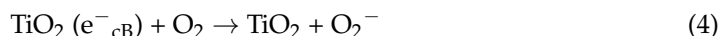
$$TiO_2 + h\upsilon\ (\lambda \geq \text{band gap}) \rightarrow TiO_2\ (h + v_B) + TiO_2\ (e^-\ c_B) \tag{1}$$

$$(h + v_B) + H_2O \rightarrow TiO_2 + H^+ + {}^\bullet OH \tag{2}$$

$$TiO_2\ (h + v_B) + {-}OH \rightarrow TiO_2 + {}^\bullet OH \tag{3}$$

$$TiO_2\ (e^-_{cB}) + O_2 \rightarrow TiO_2 + O_2{}^- \tag{4}$$

$$2O_2{}^- + 2H^+ \rightarrow H_2O_2 \tag{5}$$

$$O_2{}^- + H^+ \rightarrow HO_2{}^\bullet \tag{6}$$

$$HO_2{}^\bullet + HO_2{}^\bullet \rightarrow H_2O_2 \tag{7}$$

$$H_2O_2 + h\upsilon \rightarrow 2\ {}^\bullet OH \tag{8}$$

$$HO_2{}^\bullet + H^+ + TiO_2\ (e^-_{CB}) \rightarrow TiO_2 + OH^- + {}^\bullet OH \tag{9}$$

$$TiO_2\ (h + v_B) + \text{pollutants} \rightarrow \text{oxidation products} \tag{10}$$

$$OH + O_2{}^- + \text{water or air pollutants} \rightarrow \text{intermediate products} \rightarrow CO_2 + H_2O + \text{inorganic ions} \tag{11}$$
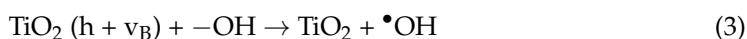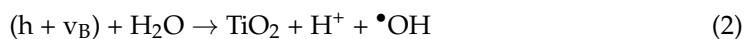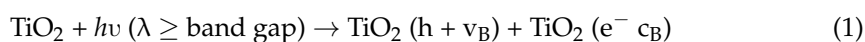

Figure 2. Schematic representation of the principle of photocatalysis on (**a**) TiO$_2$ and (**b**) N-TiO$_2$ materials.

Similarly, the photo-produced electron-hole pairs on the semiconductor's (e.g., TiO$_2$) surface have great potency in the production of H$_2$ by water splitting and reduction of CO$_2$ into fuels and various value-added chemicals. Further, the VB and CB band edge position of semiconductor nanomaterials are essential which gives information on oxidative and reductive power of photo-produced holes and elections. The CB and VB edge potential/band position must be sufficient/higher than the redox potential required for generation of higher concentration of $^\bullet$OH ($^-$OH/$^\bullet$OH = +2.4 V/NHE) and O$_2{}^-$ (O$_2$/O$_2{}^-$ = −0.33 V/NHE) radicals which could be effectively used for hydrogen production and CO$_2$ reduction reactions (Figure 3). Nevertheless, the conduction (−0.29 eV) and valence band (+2.92 eV) edge position of TiO$_2$ are not convincing enough to produce required concentrations of charge carriers [31]. Furthermore, the wide bandgap energy of TiO$_2$ (~3.2 eV) limit its light absorption to the ultraviolet light region only (~5% in solar light) and inefficient in absorption of freely available solar spectrum (~45% visible light and ~50% near infrared light). Furthermore, the poor adsorption capacity (low surface area), higher recombination rate of photo-produced charge carriers on the TiO$_2$'s surface, the morphology and the phase composition of TiO$_2$ (anatase, rutile and brookite) have significant influence on the catalytic efficiency of TiO$_2$. To overcome these, significant research efforts have been put forwarded for modification of TiO$_2$ properties by various processes which are described in the next section.
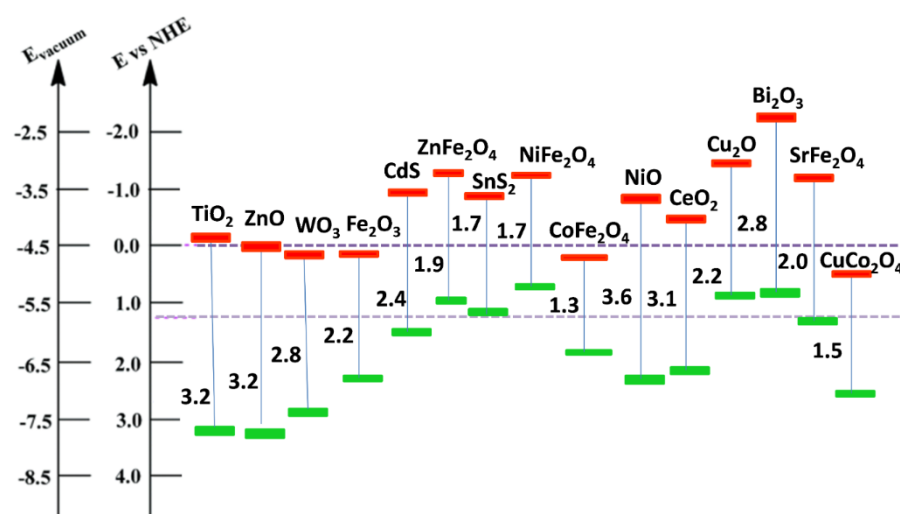
Figure 3. Band position of different semiconductors. Reproduced with permission from [31].

3. Modification of TiO$_2$ Materials and the Nitrogen Doping

Utilization of TiO$_2$ materials for complete harvesting of renewable solar (~5% UV light, ~45% visible and ~50% near infrared light) and indoor light could be performed by tuning its bandgap. In addition, the photocatalytic efficiency of TiO$_2$ could be improved by decreasing the possibility of recombination of photoproduced charge carriers, improving the surface to volume ratio, changing the ratio of anatase to rutile phase, particle size, morphology, creation and modification in the oxygen vacancy, surface modifications and trapping charge carriers and reactive radical species and other physicochemical characteristics. Thus, the tuning of bandgap and tailoring the properties of TiO$_2$ is performed by various strategies like doping with metal ions/non-metal ions, incorporation with other semiconductors and high surface area adsorbents, co-doping and surface sensitization with dyes or metal complexes or acid.

Among the modifications, non-metal ion doping into TiO$_2$, especially nitrogen-doped TiO$_2$ (N-TiO$_2$), has received significant attention because of its capability to change the surface-electronic properties that favors efficient photocatalysis. The comparable atomic size of nitrogen (155 pm) with oxygen (152 pm) can substitute the oxygen atoms from the TiO$_2$ lattice. Similarly, the ionization energy of nitrogen (first ionization energy 1402.3 kJ/mol) is comparable to the oxygen ionization energy (first ionization energy 1313.9 kJ/mol) that modifies the surface and electronic properties of TiO$_2$ and results in the enhanced photocatalytic efficiencies. Therefore, significant research has been carried out on the modifications of TiO$_2$ and various research and review articles were published on N-doped TiO$_2$ as well [9,13,32–36]. In order to obtain desired physicochemical and electronic properties various methodologies and nitrogen sources (Figure 4) have been applied for the synthesis of N-doped TiO$_2$, which are described in the forthcoming section.
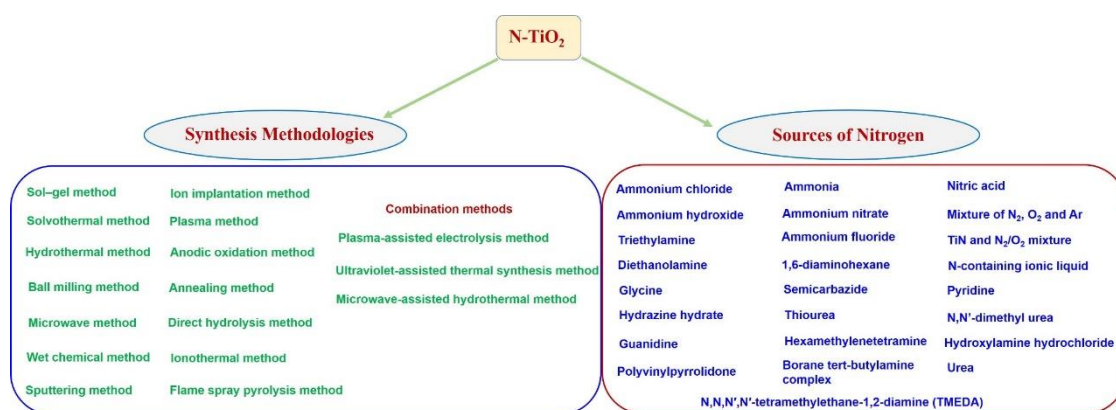
Figure 4. Methodologies and the nitrogen sources used for N-TiO$_2$ synthesis.

4. Synthesis Methodologies of N-Doped TiO$_2$

4.1. Sol–Gel Method

The sol–gel method is often regarded as a facile technique for the preparation of doped TiO$_2$ catalysts because of its process simplicity. Various types of sol–gel exist depending on the method of application. In the sol–gel method, during hydrolysis, the hydroxyl bridge is formed between the nitrogen and metal center resulting in the formation of biphasic gel structure that increases with the increase in the share of nitrogen. The main advantage of this method is the low temperature of the process, which results in the reduction of production costs as well as it does not demand any special equipment for production. Typically used precursor solution as a source of titanium includes titanium sulphate or titanium trichloride. However, other commonly used precursors for the synthesis of N-doped TiO$_2$ materials include titanium hydroxide, titanium tetrachloride and titanium isopropoxide. The sources of nitrogen include urea, hydrazine, guanidine hydrochloride, triethylamine and ammonium chloride. Avisar et al. prepared N-doped TiO$_2$ thin films by sol–gel technique using isopropanol, ammonium hydroxide, triethanolamine and tetrabutylorthotitanate precursor solutions. The sol was prepared by means of thin dip coating on the glass surface followed by air drying and calcination resulted in a crystalline thin film with anatase phase [37]. Caratto et al. synthesized N-doped TiO$_2$ nanocomposites by sol–gel method using isopropanol, titanium isopropoxide (TTIP) and ammonia solution and the presence of N^{3-} ions were confirmed through various physicochemical characterization techniques. Further, the resultant N-doped TiO$_2$ is found to show lower surface area, however, the nanocomposite is found to be more stable in the visible range [38].

4.2. Solvothermal or Hydrothermal Method

Solvothermal or hydrothermal methods are carried out under specific pressure and temperature in a hydrothermal reactor (commonly autoclave). In general, both of these methods were used to synthesize mesoporous N-doped TiO$_2$ nanocomposites. Initially, titanium and nitrogen precursors will be dissolved in either organic or aqueous medium and the resultant mixture is kept in the hydrothermal condition for several hours, thereby ending up in the formation of varied N-doped TiO$_2$ nanocomposites. Pan et al. prepared the N-TiO$_2$ hollow microspheres by the dissolution of TTIP into a propanol solution and the obtained clear solution was transformed into the Teflon-lined stainless-steel autoclave set at a temperature of 200 °C with a process time of 1 day. The resultant N-doped TiO$_2$ hollow microspheres are found to contain numerous nanothorns and small fragments of spherical shells that could be attributed to the structural collapse that might have occurred during the calcination process or could be due to the disassembly of the solvothermal reactions. The synthesized microsphere is found to have large surface area with outstanding light harvesting properties. Further, it exhibits high photocatalytic activity due to the presence of large accessible surface area that ultimately enhances the decomposition of organic

molecules [39]. Similarly, Chainarong et al. synthesized N-TiO$_2$ powders by hydrothermal method using hydrogen titanate. The mixture of TiO$_2$ powder and sodium hydroxide solution were poured into the Teflon-lined stainless-steel autoclave and maintained at 130 °C for 1 day. The nitrogen was doped into resultant synthesized TiO$_2$ by impregnation method followed by heat treatment (400 °C for 2 h). The morphology of the synthesized N-TiO$_2$ is cubic nanoparticles with length in the range of 50–500 nm. The vibration at 1430 cm^{-1} of the FT-IR spectra of the synthesized N-TiO$_2$ powders shows the presence of an O-N band that confirms that the N atom is embedded in the TiO$_2$ network. The surface area of the synthesized nitrogen-doped TiO$_2$ is found to be less than P25-Degussa and hydrothermal method synthesized TiO$_2$ (HM-TiO$_2$), however the photocatalytic activity is found to be higher under visible light than the latter two [40].

4.3. Ball Milling Method

The ball milling technique, often regarded as a mechano-chemical synthesis method, is a process where the kinetic energy of the moving balls is used to mill the material, which breaks the existing chemical bonds by fracturing the material therein resulting in the formation of fresh surface. The resultant newly formed surface containing dangling bonds is reported to be chemically reactive. Sometimes, this process could also create a high pressure/temperature exceeding several GPa/1000 °C depending upon the type of material. For instance, Yin et al. synthesized N-doped TiO$_2$ powder using hexamethylenetetramine and urea by mechanochemical method (using a planetary ball mill). As a result, it was observed that the use of mechanical treatment with high energy enhances phase conversion of anatase to rutile phase. Further, high-temperature calcination was needed to eliminate the organics from the obtained product [41,42]. Techitdheera et al. developed N-doped TiO$_2$ powders by ball milling method with variation in operating time and annealing temperatures in N$_2$ atmosphere. The results of SEM analysis of N-doped TiO$_2$ powder show high surface area with the increase in the milling time. After milling treatment and annealing with nitrogen, the crystalline structure of TiO$_2$ was identical to the structure of the TiO$_2$ precursor, which was evident from the XRD analysis. Further, the impurity phase in the TiO$_2$ precursor is found to reduce while adopting the ball milling technique with NH$_3$ (solution) and annealing with N$_2$ [43].

4.4. Microwave Method

The microwave method involves the use of microwave irradiation, an alternative energy source for catalyst preparation, under varying frequency range between 0.3 and 300 GHz (with wavelength range of 1 mm–1 m) [44]. Microwave irradiation upon a material causes disruption by thermal/athermal means. In the former, microwaves heat the material by means of molecular interaction, whereas in the latter, microwaves interact with the polar molecules therein causing disruption by various physical, chemical and biological reactions [45]. Kadam et al. carried out synthesis of N-doped TiO$_2$ nanostructure by microwave assisted method under a microwave irradiation exposure time of 20 min (900 W, 250 MHz). The synthesized N-doped TiO$_2$ nanoparticle is found to have a surface area of 140 m^2/g with high thermal stability up to 800 °C with retention of anatase phase confirmed by XRD and TEM analyses [46]. Azami et al. prepared N-doped TiO$_2$ powder with urea as N source by using microwave irradiation technique under a microwave power of 800 W with an exposure time of 30 min. The bandgap energy of the obtained N-doped TiO$_2$ was found to be 2.9 eV by UV-Vis/DRS spectrum. The results of the study reveal that N-TiO$_2$ can be formed at 230 °C with the use of microwave irradiation heating that cannot be obtained under normal conducting heating [47]. Thus, this method has desirable effect on producing dielectric heating that produces heat by means of dipole molecule rotation within the dielectric. Hence, uniform heating of the material is obtained in this technique. However, the use of this technique requires a special reactor that is needed for a microwave generator, hence it entails high instrument cost. The advantage is still the lower reaction time in comparison with the hydrothermal methods.

4.5. Wet Chemical Method

The wet chemical method involves the use of nitrogen atoms containing precursors to dope the N into TiO_2 for the preparation of highly active N-doped TiO_2 powders with visible responsible capability. Existing studies have experimented with a wide range of reagents, such as ammonia, urea, ammonium hydroxide, triethylamine, etc. of varying strength under different operating conditions. Lin et al. (2015) carried out the synthesis of N-TiO_2 by hydrolysis of TTIP using an ammonium hydroxide solution (precursor) at different concentrations with composite calcination temperatures (ranging between 300 and 600 °C) and carried out the photocatalytic activity experimentations under visible light. The results of XPS reveal that the N doped into the TiO_2 lattice and N doping is found to retard the conversion from anatase to rutile phase. Further, the maximum photocatalytic activity was observed with an ammonium hydroxide concentration of 150 mL and at a calcination temperature of 500 °C. The enhanced photoactivity relies primarily on the synthesis condition. Furthermore, the surface area of the resultant N-TiO_2 during photocatalyst preparation depends upon the nitrogen precursor used [48]. For instance, Makropoulou et al. synthesized N-doped TiO_2 by using TTIP with varying nitrogen precursors, such as ammonia, triethylamine and urea. The synthesized N-TiO_2 powder is found to have a specific surface area of 29 m^2/g while using NH_3 as precursor whereas the surface area is as low as 12 m^2/g while using triethylamine as precursor. However, the surface area of the N-TiO_2 powder synthesized using urea precursor is found to be the same as that of the self-prepared TiO_2 alone (79 m^2/g). However, the resultant N-doped TiO_2 catalysts are reported to be effective in inactivating the bacterial contaminants from the water [49].

4.6. Sputtering Method

The sputtering process is a dry process mainly adopted to prepare thin films of N-TiO_2 by means of depositing the thin film of sputtered atoms (nitrogen) onto the TiO_2 surface [50]. The type of sputtering process can be categorized according to the source of sputtering, such as ion beam, electron cyclotron resonance, direct current, etc. For the synthesis of N-TiO_2 thin films, the commonly used sputtering method includes direct current sputtering (if target is electrically conductive) and radio frequency sputtering (employed irrespective of whether the target material is electrically conductive or not) [51,52]. The sputtered atoms resulting from the sputtering process are usually ejected into the gas phase that gets deposited onto the surface within the vacuum chamber. In general, the sputtered atoms explode collision cascades in the target where an atom will be ejected if the leftover energy of the sputtered atom is greater than the binding energy of the target surface and thus sputtering happens. Dobromir et al. developed N-doped TiO_2 thin film by radio frequency (RF) sputtering method. In the study, pure Ti (99.7%) of 3.0″ diameter was used as a sputtering target under a highly pure gaseous mixture (Ar + N_2 + O_2). The prepared thin films were then subjected to an annealing treatment by successive oven heating at 400–600 °C. After this thermal treatment, the rutile crystalline phase formation was observed with the decrease in the nitrogen dopant concentration that is bounded to titanium by the substitution of oxygen that was removed by re-oxidation of the surface. Further, the results of VB XPS analysis suggest the reduction in the bandgap of N-TiO_2 with the increase of the concentration of the dopant [53]. Chan et al. prepared the N-doped TiO_2 films by reactive sputtering method on both glass and silicon substrates with air as the reactive gas to conduct the procedure at high base pressures (of about 1.3×10^{-2} Pa) in order to reduce the process time. The phase transformation of the prepared films from mixed to anatase was observed with the increase in the air/Ar flow ratio. The Tauc plots show the optimal bandgap energy of the prepared $TiO_{2-x}N_x$ films from 3.05 to 3.11 eV and falls under the visible light regime. It was observed that there is an almost linear drop in the bandgap with the rise in the N concentration in the films that is useful to improve the photocatalytic property under visible light [54].

4.7. Plasma Method

The plasma method involves the use of plasma produced by applying energy to a gas to alter the electronic structure of the atoms and to produce excited ions and species. The atmospheric plasma sources include direct current and low frequency discharge, microwave discharges, and plasma undergo ignition by means of radio frequency waves. Plasma treatments can be applied for the preparation of N-TiO$_2$ photocatalyst. In this method, the Ti-precursor solution is initially vaporized and transported by inert gas into the plasma reactor to react with excited nitrogen and thus being implanted to the vaporized TiO$_2$ particles [55]. In another way, in the plasma method, the pristine TiO$_2$ particles can be treated with the N$_2$/H$_2$ mixture or nitrogen gas to produce a yellow powder [56,57]. Yamada et al. prepared N-TiO$_2$ (surface doped) by plasma surface modification technique with argon/nitrogen plasmas, in series. The TiO$_2$ film containing Ti-N bonds produced by the substitutional N-doping demonstrates visible light activity, which is revealed by the decomposition of methylene blue while evaluating the photocatalytic activity [58]. Chen et al. synthesized N-TiO$_2$ photocatalyst by applying the atmospheric pressure plasma enhanced nanoparticle synthesis (APPENS) method. The advantage of this APPENS over other plasma techniques is operation under normal pressure and temperature and also possessing a higher rate of film deposition at comparatively low power consumption. Further, the resultant N-doped TiO$_2$ photocatalyst was more effective in toluene and isopropanol removal than the commercial P25 and ST01 (TiO$_2$ powder, Ishihara Sangyo Kaisha, Osaka, Japan) photocatalyst, and undoped photocatalysts under visible light. Thus, the APPENS process could potentially be used to control indoor and outdoor air pollutants [59].

4.8. Ion Implantation Method

The ion implantation method employs the implantation of N impurity into lattice oxygen sites of the TiO$_2$ crystal lattice, which modifies the electronic arrangement by the presence of localized states at the top of the valence band. This change would reduce the bandgap therefore enhancing the photocatalytic activity under visible light. Panepinto et al. prepared N-TiO$_2$ by N ion implantation by a dose less than 10^{16} ions/cm^2 in order to control the modification of the morphological and crystalline properties of the irradiated anatase thin films [60]. Borras et al. (2007) carried out N ion implantation by bombarding the surface of anatase TiO$_2$ thin film (at ion energy of 50 keV for varying doses of 1.2×10^{17}, 6×10^{16} and 3×10^{16} ions/cm^2) by using metal organic chemical vapor deposition (MOCVD) method. The MOCVD samples, under visible light, revealed a sharp drop in wetting contact angle from 80° to 55°. Both the films (MOCVD and non-MOCVD) attain total hydrophilicity under posterior UV irradiation [61]. Ghicov et al. (2006) synthesized N-TiO$_2$ nanotube film by N ion implantation technique by bombardment at 60 keV with a nominal dose of 1×10^{16} ions/m^2. The resultant N-doped TiO$_2$ nanotube film of crystalline anatase structure is found to have improved photocurrent response in both visible and UV range. Apart from the enhanced properties, the bombardment at this condition led to the phase conversion from anatase to an amorphous structure and hence demands subsequent thermal annealing process. This recuperates the anatase phase as well as enhances the photocurrent in both ultraviolet and visible range [62].

4.9. Direct Hydrolysis of Organic/Inorganic Salts

Direct hydrolysis involves the preparation of N-doped TiO$_2$ using an organic/inorganic salt, and usually the air/moisture sensitive alkoxide precursors under visible light. Khan et al. (2021) synthesized N-TiO$_2$ powder by a co-precipitation method using tri-thiocyanuric acid with P25 and then subsequently calcinated for 4 h at 550 °C in a nitrogen atmosphere. It was found that the N-doping increases the absorption of visible light and also enhances the transfer/separation of photo-excited charge carriers [63]. Similarly, Ji et al. (2019) prepared N-TiO$_2$ composite fibers (PAN-COOH fibers) by surface hydrolysis using PAN fibers in a sulfuric acid solution. The resultant composite fiber is found to exhibit enriched photocatalytic

capacity under UV-Vis light. However, the resultant composite fibers were found to contain mostly amorphous carbon, however there is no evidence of crystalline phase except anatase phase. Further the resultant N-TiO$_2$ composite fibers were found to have a surface area of 116.41 m^2/g, still slightly lower than that of the ordered mesoporous black TiO$_2$ with the surface area of 124 m^2/g [64].

In most of the direct hydrolysis methods, N-TiO$_2$ is either synthesized by heat treatment of pure TiO$_2$ in an NH$_3$ atmosphere or air/moisture-sensitive titanium precursors are used, which are costly and hard to handle. However, Japa et al. (2020) carried out preparation of N-doped TiO$_2$ by a thermal hydrolysis technique from TiOSO$_4$ using ammonium hydroxide (NH$_4$OH) as a source of nitrogen and a precipitating agent. In the study, authors used a cost effective, stable under air/moisture and easy to handle inorganic titanium salt (TiOSO$_4$) instead of these sensitive alkoxide precursors and hence merit real scale applications. The resultant N-doped TiO$_2$ is found to show its potency toward application in photocatalytic synthesis of fine organic chemicals in visible light. Further, the higher activity of N-TiO$_2$ in comparison with bare TiO$_2$ could be attributed to the increase in the absorption in the visible light, enhanced photoinduced charge transfer and separation [65].

4.10. Anodic Oxidation Method

The preparation of N-doped TiO$_2$ by anodic oxidation method involves two steps. Initially, the formation of oxide occurs at the metal interface by oxygen anions. Subsequently, the dissolution reaction is being initiated by the F$^-$ ions in the electrolyte. During oxide formation, the anions develop on the interface of the electrolyte through water electrolysis and these anions come into contact with the surface of the metal by diffusion. Concurrently, Ti^{4+} ions passage in the opposite direction through the oxide layer therefore reacting with oxygen anions, the TiO$_2$ formation ultimately occurs (Equation (12)). The reaction of F$^-$ ions with Ti^{4+} at the metal/oxide surface are shown in Equations (13) and (14).

$$Ti + 2H_2O \rightarrow TiO_2 + 4H^+ + 4\ e^- \tag{12}$$

$$TiO_2 + 4H^+ + 6\ F^- \rightarrow (TiF_6)^{2-} + H_2O \tag{13}$$

$$Ti^{4+} + 6\ F^- \rightarrow (TiF_6)^{2-} \tag{14}$$
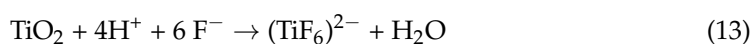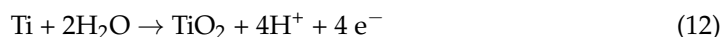
Le et al. (2018) carried out N-doping of TiO$_2$ nanotube arrays (TNA) by a two-step anodization method with NH$_4$F and glycerol-water electrolyte. The N-doping concentration varied between 0 and 9.47% by controlling the flow rate of nitrogen gas between 0 and 500 cc/min during thermal annealing at 450 °C for 3 h. The enhanced catalytic activity was detected for N-TNAs while compared to TNAs. While experimenting methylene blue degradation, it was observed that the reaction rate constant reached 0.26/h for N-TNAs, which is about 125% higher than that obtained with TNAs that showed about 0.115/h [66]. Furthermore, recent studies show that the two-step anodization method could be able to prepare highly ordered TNAs with diverse top layer morphology with increased photocatalytic and photoelectrochemical activity [67–69]. Mazierski et al. (2016) synthesized N-doped TiO$_2$ nanotube arrays by anodizing titanium foils in an organic electrolyte. The results conclude that the nanotubes synthesized with varying nitrogen concentrations of approximately the same length show differences in the crystallite size, bandgap value and Ti^{3+} state that imparts deviations in photoactivity [70].

4.11. Annealing Method

Annealing involves the thermal oxidation process at varying temperatures under an air/Ar/N$_2$ atmosphere to synthesize N-doped TiO$_2$ nanomaterials. Lai et al. (2010) developed N-TiO$_2$ nanotubes by immersion in 1 M NH$_3$.H$_2$O solution and subsequently annealed to attain the crystalline phase of N-doped TNA electrode. The resultant N-TiO$_2$ nanotubes are found to have large absorption areas with suitable potential for degradation of environmental pollutants. Further, the as-developed TiO$_2$ thin film shows an amorphous structure and hence annealing is necessary for phase transformation of the amorphous

TiO$_2$ thin film into a crystallized anatase phase [71]. Furthermore, Wan et al. (2007) fabricated rutile phase N-TiO$_2$ thin films by thermal oxidation followed by annealing TiN at a temperature above 700 °C under air atmosphere [72]. Liu et al. (2009) synthesized visible light active N-anatase TiO$_2$ sheets with dominant (001) facets derived from annealing of as-prepared TiO$_2$ nanosheet under NH$_3$ atmosphere at 400 °C. The activity observed during rhodamine B degradation with the synthesized N-TiO$_2$ nanosheet is higher than the commercial P25 TiO$_2$ particles [73].

4.12. Ionothermal Method

In 2004, Cooper et al. used the ionothermal method for the first time to synthesize crystalline zeolites using ionic liquid (1-Methyl 3-ethyl imidazolium bromide) and eutectic mixture (choline chloride/urea) as solvents and templates. The ionothermal method depends on the solvents which are predominantly ionic, because sufficient quantities of molecular water disrupt the reaction, preventing the formation of zeolites. They then termed this procedure as ionothermal synthesis to distinguish it from hydrothermal preparations, which take place in a predominantly molecular solvent [74]. Pipi et al. ionothermally prepared N-TiO$_2$ using titanium butoxide as a titanium source and choline chloride and urea (molar ratio 1:2) eutectic mixture as a solvent and source of nitrogen. Different compositions of N-TiO$_2$ were prepared by varying the percentages of the eutectic mixture, titanium butoxide, water, temperature and reaction time, and in both reflux and autoclave methods. The photocatalytic efficiency of the N-TiO$_2$ nanoparticles was determined by the oxidation of N, N-dimethyl-4-nitrosoaniline (RNO) dye in the presence of UV and visible light irradiation. Photocatalyst synthetized by the reflux ionothermal method revealed higher photocatalytic activity because of the presence of mixed phase (anatase/brookite) in N-TiO$_2$ [75].

4.13. Flame Spray Pyrolysis (FSP) Method

Flame spray pyrolysis has been used mostly for the large-scale manufacture of ceramic commodities such as titania, fumed silica, alumina and zinc oxide, respectively. FSP describes the formation of fine particles from gases in flames. Whereas, in the conventional spray pyrolysis, the aerosol droplets formation takes place by atomization of the solution in a hot wall reactor, undergoes evaporation and solute concentration within the droplet, drying, thermolysis of the precipitate particle at higher temperature to form a microporous particle, and finally a dense particle by sintering process. The advantages of FSP are the ability to dissolve the precursor directly in the fuel, simplicity in introduction of the precursor into the hot reaction zone (e.g., a flame) and flexibility in using the high-velocity spray jet for rapid quenching of aerosol formation. The schematic representation of particle formation in FSP is shown in Figure 5. Initially, the precursor material is injected into the burner as a gas, droplets or solid particles. The solid or liquid precursors are exposed to high flame temperature and rapidly evaporate into vapors that react and form intermediates, product molecules and clusters that quickly grow to nanosize particles by either coagulation, surface reactions, or both. Once the aerosol stream leaves the high-temperature zone and the temperature slowly cools down to low temperature for particle collection, particle growth takes place continuously by coagulation, though complete particle coalescence no longer occurs resulting in aggregates of primary particles [76,77].

Boningari et al. developed a visible light active N-TiO$_2$ by single-step flame spray pyrolysis (FSP) method. XPS analysis revealed that the FSP method directs the nitrogen doping predominantly in the form of interstitial nitrogen (Ti–O−N) rather than substitutional nitrogen (Ti–N). Further XRD analysis demonstrated that N-TiO$_2$ showed the distortion and strain in the crystal structure instigated by the incorporation of the nitrogen atoms. In addition, the growth or expansion of crystal lattice is due to that the atomic radius of nitrogen atoms (r = 1.71 Å) being larger than oxygen (r = 1.40 Å). The nitrogen atoms doping into the crystal structure of TiO$_2$ modifies the electronic band structure of TiO$_2$, leading to the formation of new mid-gap N 2p energy band levels above the O 2p valance

band which suppress the recombination of photogenerated charge carriers. The increased separation efficiency of charge carriers on the N-TiO$_2$ showed higher visible photocatalytic activity than the pure TiO$_2$ in degradation of phenol as a model pollutant [78].
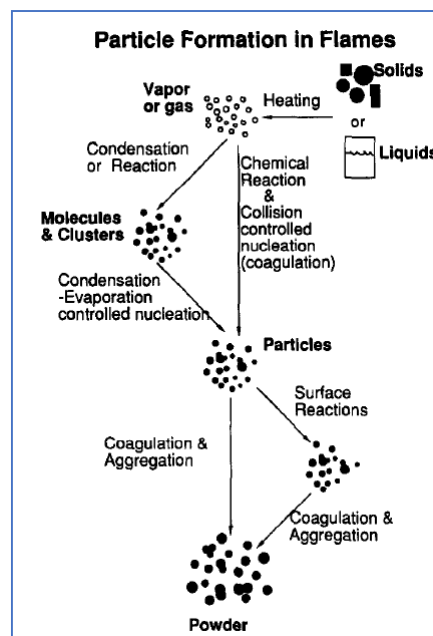

Figure 5. Schematic representation of particle formation by FSP process. Reprinted with permission from [76].

4.14. Combination Methods

4.14.1. Plasma-Assisted Electrolysis

The aforementioned methods are generally used for the synthesis of TiO$_2$ and N-TiO$_2$ with required crystal structure/phase, morphology, surface properties and particle size. However, the reaction operational parameters such as the amount of precursors, pH, nitrogen sources, reaction time and temperature must be controlled to obtain the desired properties. Furthermore, it requires high temperature and longer duration for reaction and drying the developed TiO$_2$ and N-TiO$_2$ nanoparticles, which limits the mass production of the materials and affects the practical applicability. To overcome these, Kim et al. (2018) developed a simple plasma enhanced electrolysis where the N-TiO$_2$ directly synthesized using small amount of electrolyte (nitric acid) and titanium (Ti) metal as precursors (Figure 6). The developed N-TiO$_2$ materials were calcined at different temperatures for transforming the amorphous TiO$_2$ into the crystalline TiO$_2$ anatase phase and the N-doping is an interstitial N doping state in TiO$_2$ lattices. N-TiO$_2$ nanoparticles showed superior photocatalytic ability than TiO$_2$ nanoparticle in MO dye degradation under the irradiation of visible light [79].

4.14.2. Ultraviolet-Assisted Thermal Synthesis

In this method, the ultraviolet (UV) light is used in the thermal method to assist the preparation of the photocatalytic nanomaterials in a shorter reaction time at ambient temperature and pressure. UV light is capable of initiating reactions similar to those that occur at high temperature, and the UV light energy can overwhelm the obstacle of the activation energy to disconnect the bonds and form new products. It is well known that, as per the Arrhenius law, increase in the temperature of the reactants increases the constant rate of the reaction. Further, it is well understood from the literature that the electron irradiation increases the speed of the synthetic process at low temperatures. Moreover, the UV photons change the molecule's structure by splitting of bonds and exciting the molecules into a higher level of energy, or ionization of molecules [80].
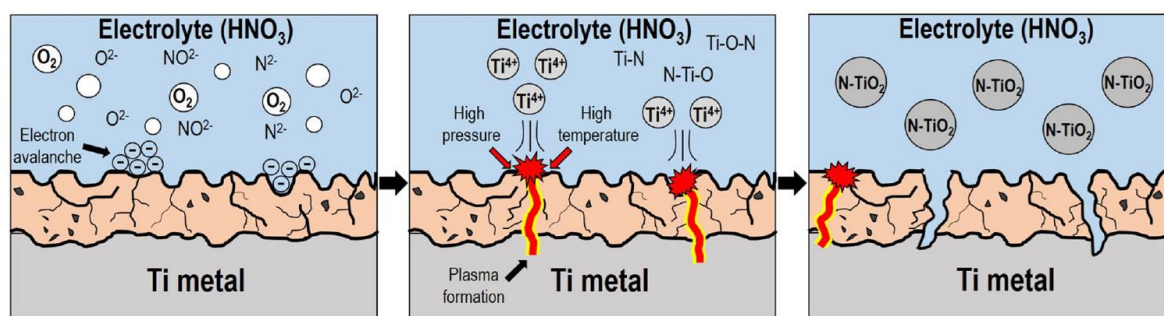
Figure 6. Schematic diagram of mechanism of N-TiO$_2$ formation via plasma-assisted electrolysis. Reproduced with permission from [79].

4.14.3. Microwave-Assisted Hydrothermal Method

As describe above, the hydrothermal method is a material synthesis method at specific temperature pressure and time, and an effective method for some materials that are insoluble at normal temperature and pressure. Furthermore, it is efficient in controlling the crystal phase, morphology and particle size of the products; therefore, it is a simple, cost-effective and environmentally friendly method. However, the hydrothermal method consumes significant amounts of time and energy. Therefore, microwave assistance, such as microwave-assisted hydrothermal method, has drawn notable attention because of its advantages, such as low reaction time, lower energy usage and materials with unique physicochemical and electronic properties. Yin et al. (2008) developed N-doped TiO$_2$ (TiO$_{2-x}$N$_y$) nanoparticles with monoclinic single phase using the microwave-assisted hydrothermal technique with hexamethylenetetramine and TiCl$_3$ as a nitrogen and titanium sources along with hydrothermal reaction temperature of 160–230 °C for 5–60 min using a microwave system (1000 W). TiO$_{2-x}$N$_y$ showed higher photocatalytic efficiency in annihilation of nitrogen monoxide in the presence of both visible-light ($\lambda > 510$ nm) and UV light ($\lambda > 290$ nm) due to the high specific surface area and fine particle size [81]. Similarly, Peng et al. (2010) prepared N-doped titanate nanotubes using the microwave-hydrothermal method at 450 W and 130 °C for 2 h followed by sintering in 20% O$_2$/80% N$_2$ atmosphere at various temperatures (250 °C, 350 °C and 450 °C for 2 h) for conversion of nanotube layers into anatase. Absorption spectra revealed that N-doped titanate nanotubes exhibit an increased absorption in the visible light regions than the bare titanate nanotube observed from the appearance of light-yellow color of the materials. This validates the N-doping results in the creation of new energy levels above the titanate nanotube VB and decreases the bandgap of the materials. N-doped titantate nanotubes showed improved photocatalytic ability over the titanate nanotube in degradation of methyl orange dye under 15 W commercial fluorescent lamps [82].

5. Possible Mechanism for N Doping in TiO$_2$

Generally, the doping of nitrogen onto TiO$_2$ in two ways, namely, substitutional or interstitial, that creates electronic mid-gaps between the band structure of TiO$_2$ that reduces the bandgap energy of TiO$_2$ and enhances the visible light photocatalytic capacity. Substitutional doping modifies the surface characteristics of TiO$_2$ whereas interstitial doping modifies the lattice structure of TiO$_2$. The pictorial presentation of the N doping (both substitutional and interstitial) is shown in Figure 7.
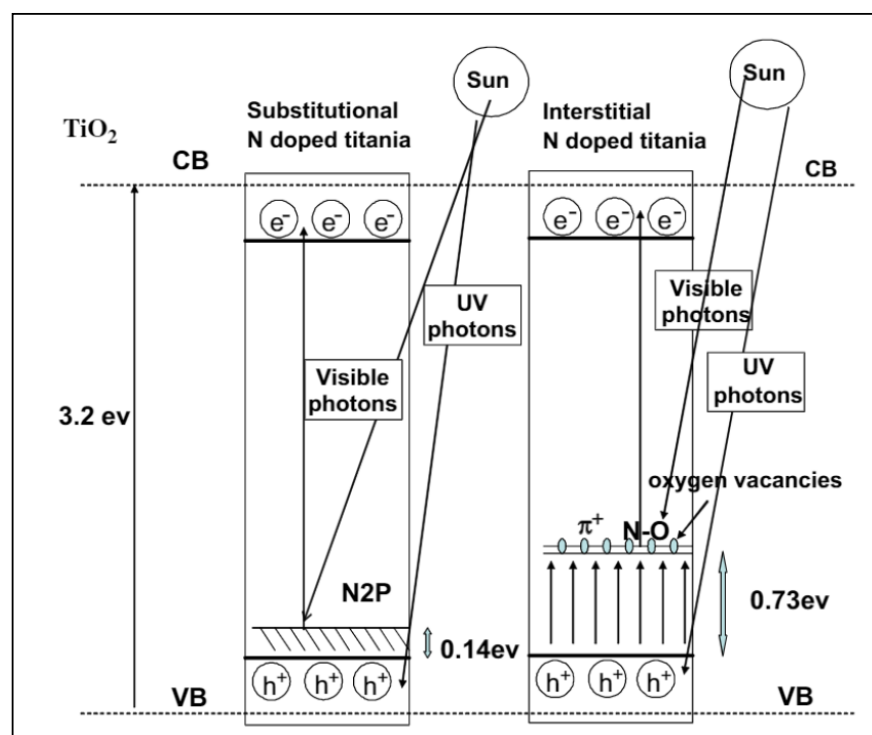
Figure 7. Electronic band structure of N-doped TiO$_2$ (both substitutional and interstitial doping). Reprinted with permission from [83].

However, the state of the N-doping into TiO$_2$ lattice and the corresponding bandgap reduction mechanism is still debatable, so, hereafter, we will describe some of the literature evidence for the possible mechanism of N doping into TiO$_2$. Asahi et al. demonstrated the state of N in TiO$_{2-x}$N$_x$ by XPS analysis, revealing that three peaks at binding energy values of 396, 400 and 402 eV, attributed to the atomic β-N (396 eV) and molecularly chemisorbed γ-N$_2$ (400 and 402 eV) [29]. Irie et al. observed N 1s peak at 396 eV, corresponded to Ti-N bonds, discovered that the oxygen sites in the TiO$_2$ lattice were substituted by the nitrogen atoms and forms an isolated narrow band above the VB and reduced the bandgap energy [84]. Similarly, Chen and Burda (2004) investigated the nitrogen incorporation into TiO$_2$ lattice using XPS analysis, revealing the O-Ti-N bond formation by nitrogen doping that was confirmed by shifting of binding energies (Ti 2p$_{3/2}$ and O 1s) to low binding energy in the XPS was observed. Ti$_{2p3/2}$ of TiO$_2$ observed at 459.7 eV and it was lowered to 458.8 eV after N doping, the lower binding energy (0.9 eV lower than the TiO$_2$) validated the N incorporation into the TiO$_2$ lattice. Similarly, in O 1s spectra, an additional peak at 532 eV is observed for TiO$_{2-x}$N$_x$ attributed to the creation of oxidized Ti-N, which leads to the Ti-O-N structure, confirming nitrogen substitution in TiO$_2$. Furthermore, N 1s (400 eV, 405 eV) and O 1s (533.5 eV) peaks for nitrogen oxides (NO and NO$_2$) are not observed on the TiO$_2$ surface, validating the formation of the Ti-O-N structure [85]. Similarly, Sathish et al. synthesized spherical shape N-TiO$_2$ through a chemical method. XRD analysis revealed an increase in the particle size and no variation in the "d" spacing values was perceived after N doping, validating that N is doped into the TiO$_2$ lattice without modifying the average unit cell dimension. In XPS, the Ti 2p$_{3/2}$ level peak for TiO$_2$ and N-TiO$_2$ materials was observed at 459.3 and 458.5 eV; the low binding energy value after N doping exhibited that the electronic interactions of Ti with N anions and the oxygen site is substituted by the N and modified the TiO$_2$ lattice. Furthermore, for N-TiO$_2$, the N 1s level exhibited a single peak at 398.2 eV corresponding to the N$^-$ anion incorporation into the TiO$_2$ lattice as N-Ti-O. Thus, it could be concluded that the status of N is anion-like (N$^-$), as well as the N-Ti-O structure in the TiO$_2$ lattice [86]. Likewise, significant research activities have been performed, however, the disputes involved in the status of N in the N-TiO$_2$ still remaining

debatable because of the change in the synthesis methodologies, nitrogen sources and other reaction operational parameters.

6. Property Evaluation of N-Doped TiO$_2$ and Its Photocatalytic Efficiency

The photocatalytic efficiency of the TiO$_2$ depends on various properties, such as crystal structure, defects, phase compositions, morphology, particle size, chemical state, bandgap values, surface area and adsorption capacity, nature of the irradiation source, electron-hole recombination behaviors on the TiO$_2$'s surface and reactive radicals' generation. It is well known that the higher bandgap values of TiO$_2$ and the physicochemical and electronic properties do not fulfil the requirements for obtaining an efficient photocatalytic activity. In order to obtain the desired properties, significant research activities are undertaken and still in progress utilizing different synthesis methodologies, various nitrogen sources and modifications in the reaction operational parameters. Herein, we tried to describe a few literature evidences for evaluating changes in the properties of TiO$_2$ after N doping and their influence on the photodegradation efficiency. For instance, Irie et al. prepared TiO$_{2-x}$N$_x$ powders with homogeneous anatase (TiO$_2$) phase by annealing the TiO$_2$ under NH$_3$ flow at different temperatures (550, 575 and 600 °C for 3 h). XPS results showed the presence of Ti-N bonds, which come from the substitution of oxygen sites by nitrogen atoms and confirmed that O-Ti-N bonds are formed. Furthermore, the TiO$_{2-x}$N$_x$ (x = 0.0050, 0.011 and 0.019) showed significant optical absorption in the visible light region. The increase in the x value results in the incremental value of visible light absorption (>550 nm), attributed to Ti^{3+} because at 550 °C the NH$_3$ decomposes into N$_2$ and H$_2$ and the H$_2$ acts as a reducing gas. TiO$_{2-x}$N$_x$ samples completely degraded the isopropanol in either UV or visible light. Furthermore, the quantum efficiency (QY) is decreased when the x value is increased, which affects the photocatalytic degradation efficiency. Therefore, irradiating the TiO$_{2-x}$N$_x$ with UV light generated higher QY values than irradiating it with visible light. This is because the oxygen sites in the TiO$_2$ lattice were substituted by N atoms forming a narrow band above the valence band. Thus, irradiating the TiO$_{2-x}$N$_x$ under UV light excites the electrons from both the VB and the narrow band, but in the presence of visible light electrons are excited from the newly formed narrow band only. Annealing of TiO$_2$ in the presence of NH$_3$ atmosphere partially replaced the oxygen sites with nitrogen atoms and simultaneously reduced the N-TiO$_2$ that causes an increase in oxygen vacancy (Vo) and the amount of Ti^{3+}. Thus, the Vo is generated below the lower end of the conduction band (0.75–1.18 eV) of anatase TiO$_2$ that acts as a recombination center for charge carriers [84]. Lee et al. developed a N-nanoporous TiO$_2$ (N-nTiO$_2$) with the mixture of anatase and brookite crystalline phases and high surface area by plasma treatment method. XRD revealed that the N-nTiO$_2$ bicrystalline structure with different bandgap energy draws attention for interfacial charge transfer (i.e., junction effect). Furthermore, the size of N-nTiO$_2$ (~18 nm) is smaller than the as-synthesized nTiO$_2$ (~28.3 nm), which could be due to the degradation of the polymer (hexadecyltrimethylammonium bromide, HTAB) network during plasma treatment. In addition, the interconnected nTiO$_2$ nanoparticles generate the nanoporous network wall, which leads to the high surface area (392.8 m^2/g: nTiO$_2$; 375.9 m^2/g: N-nTiO$_2$), pore diameter and pore volume as compared to standard TiO$_2$ and as-grown N-TiO$_2$. The surface energy determination through contact angle measurements revealed that the surface energy of N-nTiO$_2$ (245.61 mJ m^{-2}) was greater than that (78.48 mJ m^{-2}, 313%) of developed nTiO$_2$. Furthermore, the oxygen in the TiO$_2$ lattice is substituted by N through both interstitial and substitutional doping, and the photoproduced charge carrier's recombination is significantly suppressed by N doping, confirmed through photoluminescence analysis. For N-nTiO$_2$, the N-doping-induced charge-transfer transition from Vo to new energy levels occurred, which was confirmed through the shifting of emission signal to a higher wavelength (~650 nm). These improved characteristics of TiO$_2$ after N-doping showed significant enrichment in the photocatalytic ability in degradation of RhB dye (within 70 min time) and antibacterial performance

(sterilization of *Escherichia coli* (*E. coli*) and *Staphylococcus aureus* (*S. aureus*), Figure 8) as compared to standard TiO$_2$, as developed nTiO$_2$ and Ar plasma treated nTiO$_2$ [87].
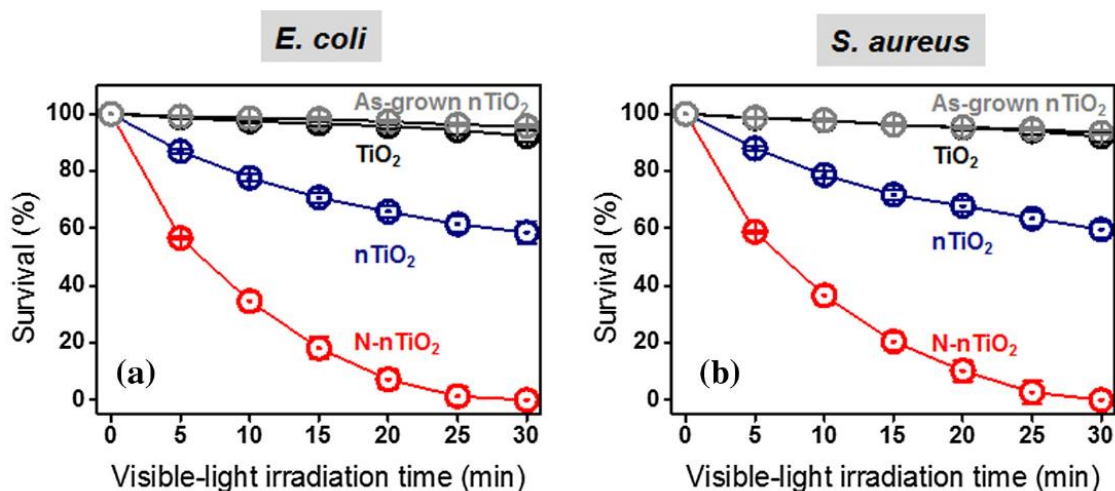

Figure 8. Antibacterial activities of TiO$_2$, as-grown TiO$_2$, nTiO$_2$ and N-nTiO$_2$ against (**a**) *E. coli* and (**b**) *S. aureus* under visible-light irradiation. Reprinted with permission from [87].

Cong et al. developed N-TiO$_2$ by a microemulsion−hydrothermal technique using triethylamine, urea, thiourea, and hydrazine hydrate as nitrogen sources. Photocatalytic activity demonstrated that the triethylamine as optimum nitrogen sources for N-TiO$_2$ synthesis and offered higher photocatalytic ability in degradation of RhB dye and 2,4-dichlorophenol than the other nitrogen-sources-based N-TiO$_2$ and undoped TiO$_2$. The N doping does not have influence on the crystal structure (i.e., retaining of anatase phase) and size, however, the particle size is reduced which was confirmed by Raman spectroscopy analysis. Furthermore, there is no change in the d-spacing value after N doping specified that N has been incorporated into the TiO$_2$ lattice without altering the average unit cell dimension. Raman spectra further revealed that the presence of peaks corresponds to vibrational characteristic band of Ti−N that validated that nitrogen substitutes some oxygen atoms in the TiO$_2$ lattice. Further, the decrease in the binding energy of Ti2p$_{3/2}$ after N doping indicates that different electronic interactions of Ti with anions occurred, leading to the partial electron transformation from the N to the Ti and an increase of the electron density on Ti was obtained because of the lower electronegativity of nitrogen compared to oxygen, which validates that N doped into the lattice and substitutes for oxygen. Thus, the chemical states of the N doped into TiO$_2$ coexist in the form of either N−Ti−O, Ti−O−N, or both. Similarly, the bandgap of TiO$_2$ is decreased from 3.04 to 2.70 eV after N-doping, which enhances the visible light absorption characteristics. The recombination of photoproduced charge carriers is significantly quenched after N doping, attributed to either trapping of electron and hole by the oxygen vacancy and the doped nitrogen or the transfer of excited electron from the valence band to the new levels introduced by nitrogen doping on the upper of the conduction band. Therefore, N doping altered the local structure of TiO$_2$ and improved the visible light absorption and separation and transfer rate of photoproduced charge carriers leading to the higher photocatalytic activity in the degradation of RhB dye and 2,4-dichlorophenol (Figure 9) [88].

Hu et al. synthesized N-TiO$_2$ by the sol–gel method using trimethylamine as N precursor and studied the influence of calcination temperature (250, 300 and 350 °C for 3 h) on the degradation of methyl orange dye. The TiO$_2$ structure changes from amorphousness to crystalline and the average nanocrystal size was increased with increasing calcination temperatures. The increase in average nanocrystal size is due to the agglomeration of nanoparticles observed during the calcination process. Furthermore, the pure anatase phase of TiO$_2$ was obtained at 300 and 350 °C calcination and the colors of these samples

changes from tan (N-TiO$_2$-250) to light gray-yellow (N-TiO$_2$-350). The N-TiO$_2$ calcined at 250 and 300 °C temperature showed higher visible light absorption due to the presence of surface organic residues whereas visible light absorption was decreased with increase in the calcination temperature. In addition, the N species doped onto the interstitial sites of the TiO$_2$ lattice, and the loss of doped N and amount of organic residues was observed with increasing the calcination temperature and the oxidized N was formed. The N-TiO$_2$ calcined at 300 °C showed low loss of doped N, small particle size, high N-doping level and low concentration of surface organic species that significantly improved the visible light photocatalytic activity in degradation of MO dye [89].
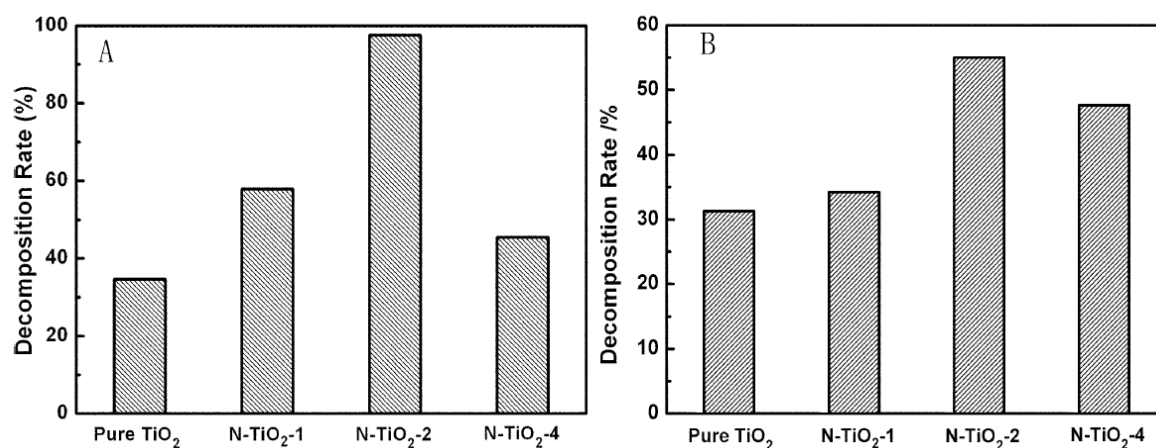

Figure 9. Decomposition efficiency of TiO$_2$ and N-TiO$_2$ with different N/Ti ratios in (**A**) RhB dye and (**B**) 2,4-DCP degradation in the presence of visible light irradiation for 1 h and 5 h time periods. Reprinted with permission from [88].

Similarly, Suwannaruang et al. observed that the high photocatalytic activity of N-TiO$_2$ depends upon the selection of nitrogen sources, and prepared a N-TiO$_2$ with nanorice grain morphology and high purity anatase phase by hydrothermal method using urea as a nitrogen precursor. When the nitrogen concentration was up to 7.5%, the nanorice grain morphology and particle size of the N-TiO$_2$ was unaltered and it was decreased to smaller size when the nitrogen concentration increased to 10 and 12.5%. The decrease in size is due to the presence of higher concentration of nitrogen in the TiO$_2$ lattice that increases the nucleation agent in the system and creates strain or stress in the system that suppresses the grain growth process. Similarly, increase in the nitrogen concentration increased the specific surface area and the average pore diameter of the N-TiO$_2$ that enhances the surface reactions. Further, the change in the shape of the pore from cylinder-shaped pore (long nanorice) to bottle shaped or slit-shaped pore (short nanorice), and the pore size distribution from broad to narrow distribution occurred. In addition, anatase to rutile phase transformation is restrained in N-TiO$_2$ that was calcined at 800 °C, whereas complete transformation to rutile phase occurred in bare TiO$_2$ materials. N doping inhibited the phase transformation (anatase to rutile) and increased the crystallite size that could be due to three reasons, namely, the use of urea delays the phase change, the three Ti-O bonds were reduced by the doped nitrogen that destroyed the connection of rutile structure and the substitution of oxygen atom in the TiO$_2$ lattice by doped nitrogen decreases the lattice distortion and accumulates strain energy indicating that the nitrogen atoms can lock the Ti-O species at the interface of the TiO$_2$. Similarly, the bandgap values of N-TiO$_2$ are increased (from 3.11 to 3.17 eV) with increase in the nitrogen concentration and lower than the TiO$_2$ material (3.20 eV). Furthermore, either substitutional (Ti–N–O . . . Ti (N) linkage), interstitial (Ti–O–N . . . Ti (N) linkage), or both N dopings occurred in the anatase TiO$_2$ lattice. The aforementioned changes in the properties of TiO$_2$ after N doping are the reasons for higher photocatalytic efficiency of N-TiO$_2$ (12.5%N) in photodegradation of ciprofloxacin under UV light as compared to other doped and commercial standard samples (anatase, rutile and Degussa P-25 TiO$_2$). The changes in the properties of N-TiO$_2$ leads to

the formation of higher concentration of hydroxyl radicals, determined using fluorescence spectroscopy during the photodegradation of ciprofloxacin using coumarin molecules as a scavenger [90]. Recently, Mirzaei et al. (2021) developed a multi-homojunction with nitrogen gradient-doped TiO_2 by pulsed laser deposition (PLD) for enhanced light absorption in the visible range and improved the charge carrier's separation and transfer efficiency through the generation of an extended band bending and an oriented electric field. Gradient nitrogen-doped TiO_2 (g-N-TiO_2) was fabricated by layer-by-layer deposition of N-TiO_2 with different concentrations of doped nitrogen on fluorine-doped tin oxide (FTO) and polished Si (100) and the thickness of each layer (~90 nm) was controlled by varying the pulse number during laser deposition. XPS analysis demonstrated that slight shift in the Ti2p peak's position attributed to the partial replacement of nitrogen with oxygen occurred, which increases the electron density on Ti. Furthermore, it is demonstrated that increasing the $N_2:O_2$ ratio during PLD revealed substitutional N doping. The developed g-N-TiO_2 is a complete anatase crystal structure, with no additional peaks that could be due to the controlled substitutional N doping without either phase change, the low concentration of N doping, or both, in the structure. Higher visible light absorption (lower energy) was observed in higher concentration of the N doping (50–90%) with substitutional doping and the bandgap of TiO_2 was decreased to 2.6 eV. Furthermore, the g-N-TiO_2 showed slight lower light absorption than the N-TiO_2 sample; however, the g-N-TiO_2 exhibited higher photocatalytic activity compared to TiO_2 and N-TiO_2 samples. This enhancement in the photocatalytic activity is mainly due to the enhanced separation and transfer efficiency of photo-generated charge carriers by the formation of homojunction with terraced band bending. Therefore, it is confirmed that the doping of N introduces an acceptor level above the valence band of TiO_2 and lowers the Fermi level (E_F) of TiO_2 and the band bending occurs when different layers (with different E_F) are brought into contact. However, it is limited in non-gradient-doped N-TiO_2 and showed low separation efficiency. Furthermore, the formation of terraced valence band levels for different layers in g-N-TiO_2 occurred that trigger a built-in electric field perpendicular to the substrate that enables the transfer of charge carriers by repelling them in different directions along the vertical direction of columnar-like structure of the g-N-TiO_2. Therefore, the g-N-TiO_2 demonstrated a superior photocatalytic performance in sulfamethoxazole removal compared to the pristine and conventional nitrogen-doped TiO_2 (non-gradient) [91]. Similarly, significant research has been performed on the synthesis of N-doped TiO_2 and the evaluation of structural, textural and electronic properties and their influence on photocatalytic efficiency.

7. Co-Doping into N-Doped TiO_2

Co-doping is another approach for enhancing the visible light photocatalytic capacity of N-doped TiO_2 by coupling with other metal or non-metal ions and semiconductor nano-materials for improving visible light absorption and adsorption capacity and suppressing the recombination of photogenerated charge carriers. Generally, the improvement in the visible light absorption and suppression of charge carrier recombination after co-doping can occur via two pathways, namely, generation of new energy levels in between the Ti 3d states of the conduction band and the O 2p states of the valence band or the co-doping compensates the addition charge created by the presence of N^{3-} in TiO_2, thereby reducing the charge carrier's recombination centers and increasing the amount of dopant. Significant studies have been carried out on the co-doping of N-TiO_2 and showed efficient photocatalytic activity. However, it is rather difficult to conclude which co-dopants are better at improving the photocatalytic efficiency of N-TiO_2 because of the variations in the synthesis and experimental operational parameters, and the properties of N-TiO_2. Therefore, this section describes the various metals, non-metals and nanomaterial-based co-dopants for improving the photocatalytic activity of N-TiO_2.

Rani et al. prepared Ni-N-TiO_2 nanoparticles using the sol-gel method. They observed that the introduction of dopants (nickel and nitrogen) generates impurity levels of Ni 3d below the Ti 3d conduction band and N 2p above the O 2p valence band that causes signifi-

cant effort in decreasing the bandgap of TiO_2, which leads to the transfer of electrons from VB to CB taking place (Figure 10). In addition, the average crystalline size of the materials is decreased which enhances the surface area of the doped materials. The enhancement in the surface area and decrease in the bandgap energy showed significant visible light catalytic activity in congo red (CR) and methyl orange (MO) dye degradation [92].
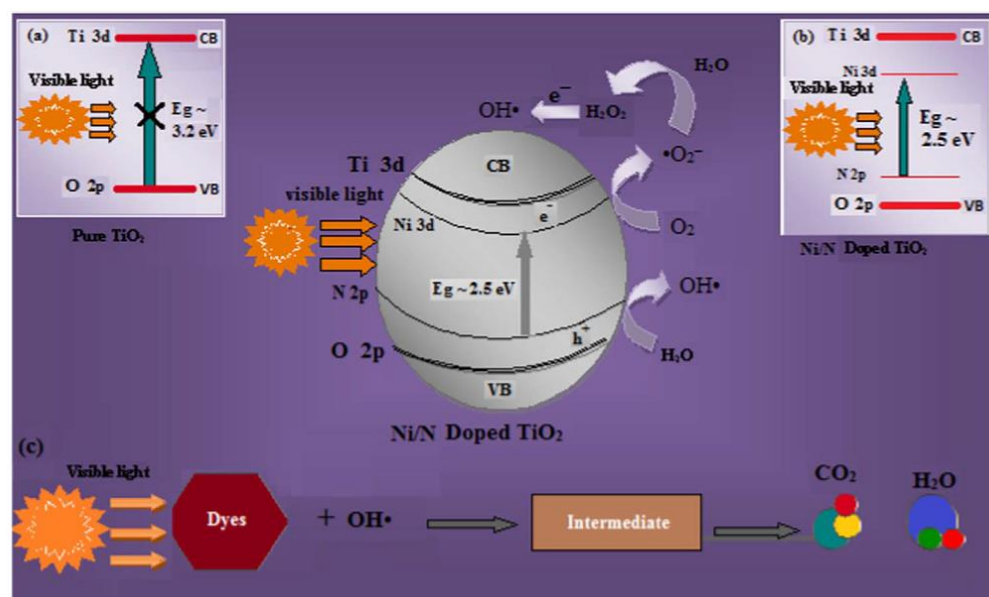

Figure 10. Schematic representation of photogenerated electron-hole pairs separation and transport process on (**a**) pure TiO_2 and (**b**) Ni-N-co-doped TiO_2 nanoparticles under visible light irradiation for (**c**) degradation of dyes. Reprinted with permission from [92].

Alotaibi et al. developed Zn and N co-doped TiO_2 thin films on glass substrates using aerosol-assisted chemical vapor deposition and evaluated their influence on superoxide formation, catalytic activity and bactericidal properties. Superoxide formation from metal oxides was determined using 2,3-Bis(2-methoxy-4-nitro-5-sulfophenyl)-5-[(phenylamino)carbonyl]-2*H*-tetrazolium sodium salt (XTT) and an increased concentration of superoxide formation from the Zn, N: TiO_2 thin films. Similarly, the transient absorption spectroscopy study revealed that photogenerated charge carrier populations were increased when films were co-doped with Zn and N and showed efficient photocatalytic activity and bactericidal activity in degradation of stearic acid and *E. coli* under UVA and fluorescent light (Figure 11, asterisk symbol) [93].

Selcuk et al. synthesized N-TiO_2 by hydrolysis method and the metals, such as Fe, Cr, Ni and Pt, were deposited onto the N-TiO_2 by reduction of the respective metal salts. The hydrogen production reaction revealed that both Pt-N-TiO_2 (11,620 µmol) and Ni-N-TiO_2 (2946 µmol) showed higher water splitting efficiency than the other metal-doped N-TiO_2, N-TiO_2 and TiO_2 materials in aqueous methanol solution. Subsequently, Ni–N–TiO_2 was selected as a suitable alternative to Pt-N-TiO_2 and a detailed study was carried out on the Ni co-doped N-TiO_2 with different nickel concentrations. Ni–N–TiO_2 with 10 µmol Ni/g N–TiO_2 exhibited higher water splitting efficiency (490 micromoles H_2 g^{-1}_{cat} h^{-1}) than the other Ni concentration doped N-TiO_2 [94]. Similarly, Lin and Shih (2015) developed metal ions (M = Cr, Ni, Cu, Nb) and nitrogen co-doped TiO_2 photocatalysts through one-pot microwave-assisted hydrothermal method. They observed that the doping of metal ions introduced donor levels in the bandgap of $TiO_{2-x}N$, which mainly occurs through the hybridization between 3d orbital of metal dopants, 2p orbital of nitrogen and associated charge compensation vacancies in M-doped $TiO_{2-x}N_y$. Among the co-dopants, Cu/$TiO_{2-x}N$ exhibited higher photocatalytic activity in hydrogen production under UV (27.4 mmol g^{-1} h^{-1}) and visible light (283 µmol g^{-1} h^{-1}) irradiation from aque-

ous methanol solution. The higher photocatalytic activity is due to the enhanced visible light absorption (introduction of new donor levels), uniform dispersion of copper ions inside the mesoporous $TiO_{2-x}N$ network and the photogenerated charge carrier's separation and transfer efficiency [95]. Abdelraheem et al. hydrothermally synthesized anatase nitrogen and boron co-doped TiO_2 (N-B-TiO_2) using borane tert-butylamine complex as a source for N and B for degradation of bisphenol A (BPA) in the presence of visible light irradiation. All N-B-TiO_2-doped samples exhibited higher photocatalytic activity than the pure TiO_2 and N-TiO_2 materials and fitted with pseudo-first-order kinetics. The results demonstrated that 2% loaded showed higher photocatalytic performance than the catalytic system used in the study (Figure 12). Furthermore, the influence of various operational parameters (initial BPA concentration, calcination temperature, dopant concentration) on the degradation of BPA were also studied [96].
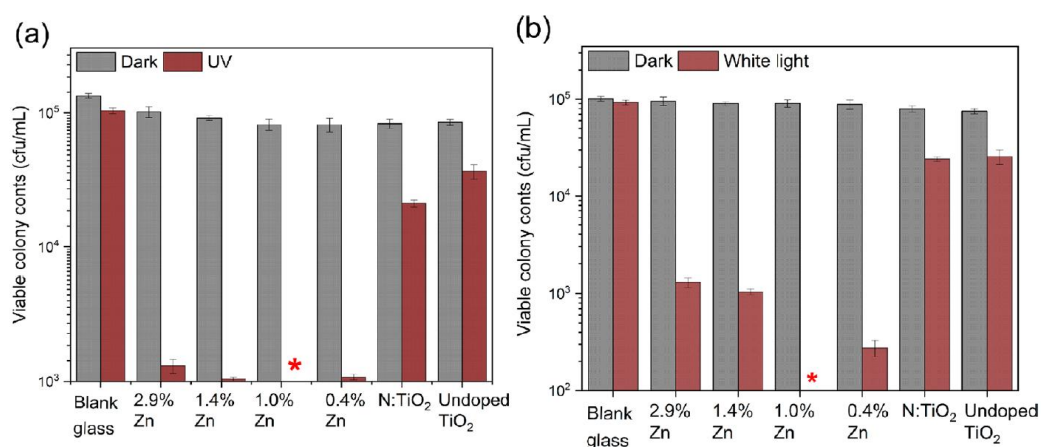

Figure 11. Bactericidal activity of the undoped TiO_2, N:TiO_2 and the series Zn, N:TiO_2 catalyst in the presence of (**a**) UVA (8 h) and (**b**) fluorescent light (18 h) irradiation. Reprinted with permission from [93]. Asterisk showed the highest bactericidal activity of Zn, N: TiO_2 thin films (1%) under both UVA and fluorescent light irradiation.
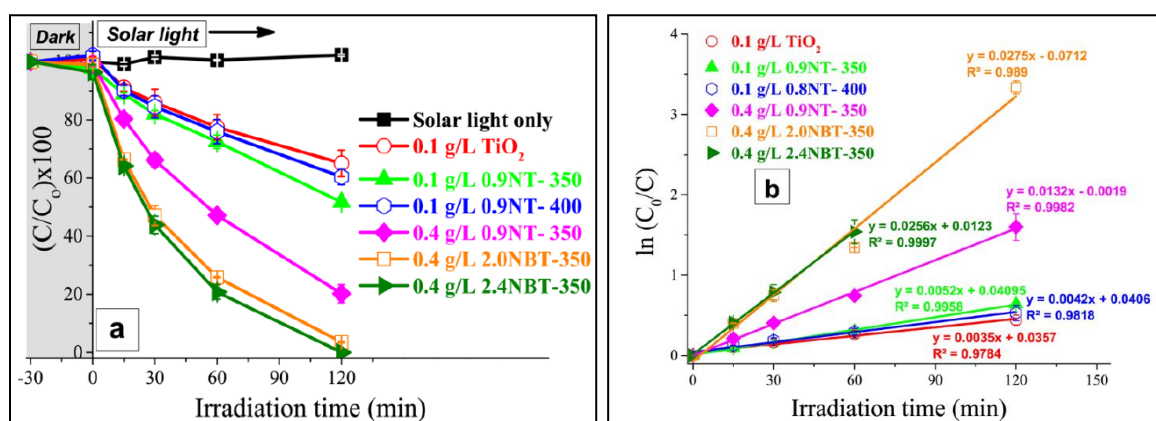
Figure 12. Photocatalytic degradation efficiency (**a**) and pseudo-first-order kinetics fitting (**b**) of BPA degradation. Reprinted with permission from [96].

Similarly, they used the same materials for degradation of pollutants such as BPA, ibuprofen (IBP), triclosan (TCS), diclofenac (DCF) and estrone (E1) spiked in Milli-Q water and different wastewater (microfiltration effluent, secondary-treated wastewater and reverse osmosis permeate from GWRS facility at Orange County, CA, USA) samples in the presence of visible light irradiation. The degradation reaction was performed using individual compounds and quinary mixture of pollutants. The results revealed that N-

TiO$_2$ showed higher degradation efficiency of pollutants in a single system compared to the quinary degradation system. The order of degradation efficiency is DCF > E1 > BPA~IBP > TCS, the difference in efficiency is attributed to their different affinities towards reactive oxygen-based species (ROS, $^1O_2$, $O_2^{\bullet-}$, HOO$^{\bullet}$ and $^{\bullet}$OH), especially $^{\bullet}$OH. Therefore, the role of ROS in pollutant decomposition is higher than the affinity of pollutants towards N-B-TiO$_2$ catalyst surface because of the low adsorption of pollutants onto the N-B-TiO$_2$ surface. They also studied the influence of the presence of inorganic ions (i.e., NO$_3^-$, Cl$^-$, Br$^-$, HCO$_3^-$) on the degradation efficiency and identified the possible intermediates formed during degradation of pollutants [97]. Similarly, significant research activities have been performed, therefore Table 1 summarized a few of the co-doped N-TiO$_2$ photocatalytic systems.

Table 1. Summary of the few co-doped N-TiO$_2$ based photocatalytic systems for degradation of pollutants.

Catalyst	Synthesis Method	Nitrogen Source	Applications	Process Condition	Catalytic Efficiency	Ref.
N-xFe-TiO$_2$	Precipitation-Hydrothermal Method	Ammonium Chloride	RhB	Conc.: 20 mg/L, Vol.: 50 mL, 300 W HPMV Lamp (UV), 1000 W Halogen Lamp (visible)	N-0.5Fe-TiO$_2$-75% (visible) and 5% (UV)	[98]
C-N-TiO$_2$ C$_x$−N$_y$−TiO$_2$	Sol–Gel	Urea	Methylene Blue (MB)	Conc.: 1.8×10^{-5} M, Vol.: 100 mL, 150 W Xe Arc Lamp	C-N-TiO$_2$ Higher Activity than the N-TiO$_2$, C-TiO$_2$ and TiO$_2$	[99]
Ce-N-TiO$_2$ Ti$_{1-x}$Ce$_x$O$_{1-y}$N$_y$	One-Step Modified Technique	Urea	MB	Conc.: 15 mg/L, Vol.: 50 mL, 30 W Fluorescent Lamp (365, 420, 500, 550, 600 nm)	Ti$_{0.993}$Ce$_{0.007}$O$_{2-x}$N$_x$ (x = 0.0070) NPs Higher Activity than the Bare TiO$_2$	[100]
N,W Co-Doped TiO$_2$	Solution Combustion Method	Urea	Rhodamine B (RhB)	Conc.: 25 µM, Vol.: 20 mL, 300 W Xe Arc Lamp	TiO$_2$: N–W (1.5%) Showed 14 Times Higher Activity than the P25 and Bare TiO$_2$	[101]
N/Pd-TiO$_2$	Modified Sol–Gel Method	Ammonium Hydroxide	Eosin Yellow	Conc.: 15 ppm, Vol.: 100 mL, 150 W Xe Arc Lamp	N/Pd-TiO$_2$ (0.6% Pd)-Complete Degradation	[102]
Ag-N-TiO$_2$	Sol–Gel-Microwave Chemical Method	Urea	MB	Conc.: 10 mg/L, Vol.: 50 mL, 30 W Fluorescence Lamp	93.44% (Ag-N-TiO$_2$ 39.40% (P25)	[103]
Cu-N-TiO$_2$	Sol–Gel	Triethylamine	MB and p-Nitrophenol (PNP)	Conc.: 0.01 mM (MB), 10 ppm (PNP), Vol.: 50 mL, 150 W Xe Lamp	2at.%Cu–3at.%N–TiO$_2$: 100%, MB and 45% PNP	[104]
Mesoporous C and N-co-doped TiO$_2$	One-Pot Hydrothermal	Glycine	Ibuprofen	Conc.: 20 ppm, Vol.: 220 mL (UV), 200 mL (Vis), 150 W HPMV (UV), LED Lamp (420 nm)	98.9% (N-TiO$_2$, UV), 100% (visible)	[105]
Anatase B and N- TiO$_2$	Hydrothermal	Three Different Borane Tert-Butylamine Complex	Bisphenol A	Conc.: 1 µM, Vol.: 400 mL, 500 W Xe Lamp	100% (2.0%NBT-350)	[96]
Sm and N- TiO$_2$	Sol–Gel Process and Ultrasound Assisted Sol–Gel Process	Urea	4-acetamidophenol (4-AMP)	Conc.: 50 ppm, Vol.: 50 mL, 300 W UV and Incandescent Lamp (>420 nm)	87% (photo with ultrasound) and 91% (photo with hydrodynamic Cavitation)	[106]

Table 1. *Cont.*

Catalyst	Synthesis Method	Nitrogen Source	Applications	Process Condition	Catalytic Efficiency	Ref.
Mn and N-TiO$_2$	Cavitation Induced Synthetic Greener Methodology	Hydroxylamine Hydrochloride	Quinalphos and 2-Chlorophenol (2-CP)	Conc.: NA, Vol.: 50 mL, LED Lamp (660, 565 and 490 nm)	87.5% (quinalphos), 91.7% (2-CP) with 660 nm LED Lamp	[107]
N-Ni-TiO$_2$	Sol–Gel	Diethanolamine	1,4-Dioxane Degradation and H$_2$ Production Simultaneously	Conc.: NA, Vol.: NA, Visible Light	N-Ni-TiO$_2$ Showed Higher Activity than the TiO$_2$	[108]

NA—data not available.

8. N-TiO$_2$ Based Z-Scheme Heterojunction System

In order to enhance the photocatalytic activity of N-TiO$_2$, the Z-scheme type heterojunction system was developed by integrating the N-TiO$_2$ with another semiconductor nanomaterial. The Z-scheme type materials classified as direct system where the redox-mediator is not used, whereas in the case of indirect system the Z-scheme is formed through various redox-mediators (e.g., IO$_3^-$/I$^-$, Fe^{3+}/Fe^{2+}). The Z-scheme system increases the visible light response of N-TiO$_2$ and the photogenerated electron and hole pairs are efficiently separated in the CB and VB of the two different semiconductors which leads to enhancement in the photocatalytic efficiency. The Z-scheme system has been used for the degradation of water pollutants, however, the experimental evidence for the Z-scheme mechanisms is ambiguous and has not been investigated deeply. Furthermore, the Z-scheme describes only thermodynamically uphill reactions (e.g., water splitting reaction), whereas the photocatalytic degradation of pollutants is thermodynamically downhill reactions. Therefore, the usage of Z-scheme in photocatalytic degradation application might create scientific misconception and detailed explanation is given in references [109,110]. Therefore, the water splitting application of N-TiO$_2$-based Z-scheme-type systems is described hereafter. Nakada et al. developed a Z-scheme system using RuO$_2$-modified rutile TiO$_2$:Ta/N (as an O$_2$ evolution photocatalyst), Ru-loaded SrTiO$_3$:Rh (as an H$_2$ evolution photocatalyst) and an Fe^{3+}/Fe^{2+} redox couple for water splitting in an aqueous NaIO$_3$ solution under visible light ($\lambda > 420$ nm) and AM 1.5G simulated sunlight irradiation. In the presence of visible light irradiation, Z-scheme transfer of photogenerated charge carriers occurred between two different photocatalysts that leads to the continuous and simultaneous evolution of O$_2$ and H$_2$ (Figure 13) [111].

Similarly, they prepared a co-catalyst-free visible-light-driven Z-scheme water-splitting system by combining N/F-co-doped rutile TiO$_2$ (as an O$_2$-evolution photocatalyst) with Ru/SrTiO$_3$:Rh (as an H$_2$-evolution photocatalyst) and [Co(bpy)$_3$]$^{3+/2+}$ (bpy = 2,2′-bipyridine) redox mediator. In the initial stage of light irradiation, O$_2$ evolution occurred because of the absence of [Co(bpy)$_3$]$^{3+}$ and the continuation of irradiation leads to formation of [Co(bpy)$_3$]$^{3+}$ which leads to the steady O$_2$ evolution on N/F-co-doped rutile TiO$_2$ and the H$_2$ evolution on Ru/SrTiO$_3$:Rh materials. The photogenerated charge carriers are efficiently separated in the CB and VB of the two different semiconductors through the redox mediators, eventually the continuous evolution of O$_2$ and H$_2$ was observed and showed two times higher activity than the RuO$_2$-modified rutile TiO$_2$:Ta/N system [112].
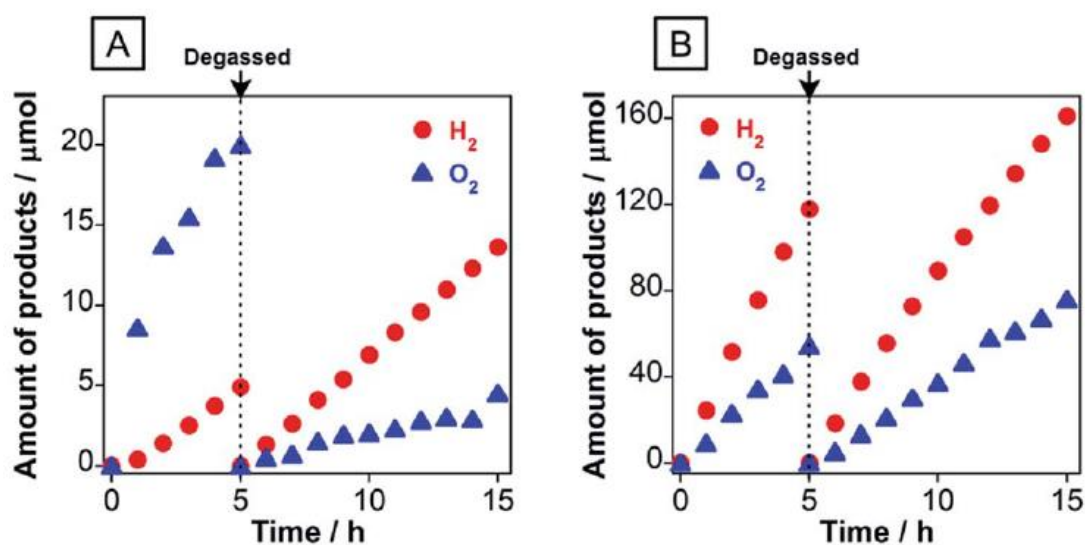
Figure 13. Photocatalytic H_2 and O_2 evolution using RuO_2/TiO_2:Ta/N and Ru/SrTiO3:Rh in an aqueous solution containing (**A**) $NaIO_3$ (1 mM) and (**B**) $FeCl_3$ (1 mM) under visible-light irradiation. Reprinted with permission from [111].

9. Visible Light Photocatalysis of N-Doped TiO_2

Nitrogen doping into TiO_2 effectively increases the visible light absorption (i.e., reduces the bandgap energy) and suppresses the rapid recombination of photogenerated electron hole pairs that significantly improves the photocatalytic capacity of TiO_2 in the presence of visible light irradiation. In addition, the phase composition, surface area, morphology and defects in N-TiO_2 also play a vital role in enhancing the visible light photocatalytic activity. Therefore, various literature is available on the development of N-TiO_2 that has mainly been used for the degradation of pollutants, renewable energy production (i.e., water splitting), CO_2 reduction, antibacterial, photoreforming of wastewater, sensors, solar cells and organic transformation applications. This review article mainly focuses on summarizing the photocatalytic application of N-doped TiO_2 towards pollutant degradation and water splitting applications.

9.1. Pollutants Degradation

Photocatalytic degradation capacity of N-TiO_2 has been majorly studied for the degradation of pollutants in both the aqueous and gaseous phase under visible light irradiation. Photocatalytic degradation application of N-doped TiO_2 was first evaluated by Sato; NOx-doped TiO_2 was prepared by calcination of titanium hydroxide and utilized for oxidation of carbon monoxide and ethane and by oxygen isotope equilibration in the presence of visible light irradiation [28]. Asahi et al. prepared $TiO_{2-x}N_x$ thin films by sputtering method and evaluated its catalytic activity by degradation of methylene blue and gaseous acetaldehyde in the presence of visible light irradiation (wavelength <500 nm). $TiO_{2-x}N_x$ exhibited higher photocatalytic activity than the bare TiO_2 under visible light irradiation, however, it exhibited similar activity under UV light [29]. Burda et al. reported a room temperature synthesis of $TiO_{2-x}N_x$ by direct amination of TiO_2 nanoparticles using triethylamine, the color of TiO_2 changed to yellow after nitrogen doping, which showed significant optical response in the visible light range. The photocatalytic activity demonstrated that $TiO_{2-x}N_x$ showed higher catalytic activity than the TiO_2 system in the degradation of MB dye under irradiation of 390 and 540 nm visible light using a laser system (Clark MXR 2001 femtosecond) [113]. Nosaka et al. prepared N-TiO_2 by calcination of TiO_2 powder with organic nitrogen compounds (urea, guanidine hydrochloride, guanidine carbonate) at various temperatures (350, 450 and 550 °C). Two kinds of N signals were obtained in XPS analysis of N-doped TiO_2, which contributes to the visible light absorbance. XPS signals at 396 eV and 400 eV assigned to Ti-N (substituted N atom for the O site in TiO_2

lattice) and N–O, respectively. The results demonstrated that the absorption edge of TiO_2 powder is significantly extended towards visible light irradiation, and N-TiO_2 prepared by guanidine showed higher visible light absorbance than urea, showing that a higher amount of nitrogen was doped with guanidine. However, the N-TiO_2 prepared by urea exhibited higher degradation efficiency in degradation of 2-propanol than that prepared with guanidine hydrochloride which indicates that high visible light absorption does not correlate with the photocatalytic activity. So, the higher photocatalytic activity is due to the substituted N atom for the O site in TiO_2 lattice and N–O have negative impacts on visible light photocatalytic activity [114]. Kalantar et al. utilized the ultrasonic assisted direct impregnation method for preparation of N-TiO_2 using urea as nitrogen source. Crystallite size of TiO_2 (21 nm) is decreased after nitrogen doping (19 nm, N-TiO_2), which results in higher surface area (63 m^2/g) than the TiO_2 nanoparticle (50 m^2/g). Furthermore, the ionic radius of N^{3-} (0.171 nm), which is close to that of O^{2-} (0.144 nm), could be incorporated into the TiO_2 lattice that weakens the crystalline phase stabilization, causes lattice distortion that leads to decrease in the crystallite size and enhancement in the surface area. The increase in the surface area is due to the ultrasonic irradiation that produces cracks and creates porous structure on the TiO_2 particle and also prevents the agglomeration of nanoparticles. This showed higher visible light activity than the TiO_2 in oxidative desulfurization of dibenzothiophene in a diesel fuel model under visible light irradiation and air bubbling. Furthermore, the enhancement in the photocatalytic activity is because of the effective separation of photogeneration of electron hole pairs through new N 2p energy levels formed above the valence band of the TiO_2 [115]. Ramezani Sani et al. developed N-TiO_2 nanowires using an annealing method under nitrogen atmosphere at different temperatures. N-TiO_2 nanowires exhibited the presence of both anatase and rutile phases of TiO_2 and significant enhancement in the visible light absorption was observed leading to higher visible light photocatalytic activity in methyl orange dye degradation than the TiO_2 nanowires [116]. Bakre et al. studied the influence of nitrogen sources on the photocatalytic activity of N-TiO_2 under natural sunlight irradiation. N-TiO_2 prepared by decomposition of urea, semicarbazide and N, N′-dimethyl urea precursors, and the nitrogen doping occurred on the TiO_2 lattice. The N-TiO_2 prepared using semicarbazide precursors showed higher photocatalytic activity in degradation of MB and RhB dye compared to other precursor-based N-TiO_2 and the standard Degussa P-25 TiO_2 catalyst. The optimal nitrogen doping, anatase–rutile coupling, smaller size, large surface area, efficient suppression of charge carrier's recombination and the presence of more surface hydroxyl groups are responsible for the higher photocatalytic degradation efficiency [117]. Huang et al. developed a N-TiO_2 material with abundant and tunable oxygen vacancies using a hydrothermal method followed by calcination in NH_3 atmosphere. The photocatalytic efficiency of the N-TiO_2 was evaluated by the degradation of rhodamine B dye (10 mg/L) and tetracycline antibiotic (20 mg/L) in the presence of visible light irradiation. The N-TiO_2 showed superior visible light photocatalytic activity than the bare TiO_2. The superior activity is attributed to the existence of new N 2p energy levels formed between the CB and VB after N doping and the rich oxygen vacancies that enhance the visible light absorption and inhibit the recombination of photogenerated electron hole pairs (Figure 14) [118].
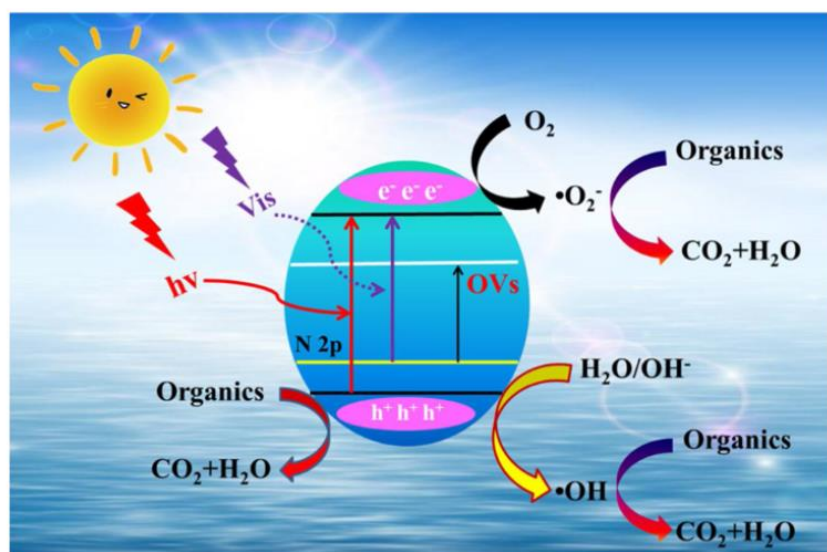
Figure 14. Schematic representation of photocatalytic mechanism of RhB and TC degradation using N-TiO$_2$. Reprinted with permission from [118].

Similarly, Zeng et al. prepared N-TiO$_2$ using precipitation combined with a thermal decomposition method using urea (CO(NH$_2$)$_2$, U), ammonium chloride (NH$_4$Cl, AC) and ammonium nitrate (NH$_4$NO$_3$, AN) as a nitrogen source, for the degradation of flumequine (FLU) antibiotic under visible light irradiation. All three nitrogen-source-based N-TiO$_2$ showed higher photocatalytic performance than the pure TiO$_2$; the order is TiO$_2$/AN > TiO$_2$/AC > TiO$_2$/U (Figure 15a). The apparent first-order rate constants (*k*app) for FLU degradation in the presence of TiO$_2$/AN catalyst are about 35, 16 or 1.4 times higher than that of pure TiO$_2$, TiO$_2$/U or TiO$_2$/AC, respectively (Figure 15b). The superior photocatalytic activity of TiO$_2$/AN sample attributed to the presence of two different valence states of nitrogen (N^{5+} and N^{3-}) in this catalyst captures the photoproduced electrons, resulting in the reduction of recombination rate of the photogenerated electron and hole pairs [119].
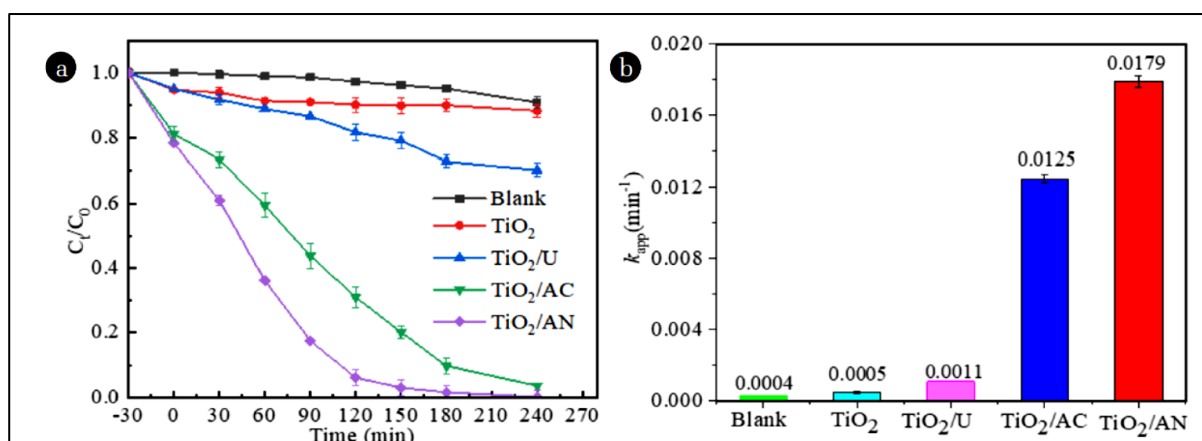

Figure 15. Photocatalytic FLU degradation efficiency (**a**) and its kinetic constant value (**b**) using TiO$_2$, TiO$_2$/AN, TiO$_2$/AC and TiO$_2$/U catalyst under simulated sunlight irradiation. Reprinted with permission from [119].

In addition to properties of TiO$_2$, the nature of the irradiation sources also have significant influence on enhancement in the photocatalytic activity of N-TiO$_2$ photocatalyst. Tryba et al. prepared N-TiO$_2$ photocatalyst by a sol–gel method using ammonia as nitrogen source and the synthesized materials are calcined at 200 to 500 °C for 1 h. The photocatalytic activity was evaluated by the degradation of acetaldehyde under UV and visible light

(fluorescent lamp) irradiation. The results demonstrated that all the N-TiO$_2$ samples showed lower catalytic activity than the undoped TiO$_2$ and the N-TiO$_2$ calcined at 300 °C exhibited higher efficiency among the calcined materials. The fluorescent lamp comprises of large region in the visible spectrum but the presence of small part of UV light caused TiO$_2$ samples to not have any significant visible light photocatalytic activity. The blank test in the presence of a fluorescent lamp exhibited 8.5% acetaldehyde decomposition, which clearly shows that UV activity of TiO$_2$ was greater than the visible light activity [120].

Similarly, after Sato and Asahi et al., inventive N-TiO$_2$ were also used for the degradation of various gaseous pollutants in the presence of visible light irradiation. For example, Li et al. synthesized yellow colored N-TiO$_2$ by spray pyrolysis method using mixed solution of TiCl$_4$ and nitrogen precursors (urea, guanidine or ammonium fluoride). Among the precursors used, N-TiO$_2$ prepared from ammonium fluoride exhibited higher photocatalytic activity towards acetaldehyde and trichloroethylene degradation than the other nitrogen-sources-based N-TiO$_2$ and standard Degussa P25 TiO$_2$ under visible light irradiation. The enhancement in the photocatalytic activity is attributed to high surface area, co-doping of F along with N doping onto TiO$_2$ that enhances the visible light absorption and surface acidity. In addition, N doping created oxygen vacancies that enhance the visible photocatalytic activity, however, the comparison showed that the degradation efficiency is less significant than the co-doping of F, surface acidity and area [121]. Aoki et al. developed N-TiO$_2$ by annealing the anatase TiO$_2$ and urea in air, followed which the N-TiO$_2$ was coated onto the glass plate for the degradation of formaldehyde and toluene mixtures in the presence of visible light. The N-TiO$_2$ surface showed hydrophilic nature exhibiting preferential adsorption of hydrophilic formaldehyde than the hydrophobic toluene and revealed higher degradation efficiency towards formaldehyde than the toluene in the mixtures. Thus, when the N-TiO$_2$ is applied for purification of indoor air, the degradation of hydrophilic pollutants is suppressed by the presence of hydrophobic pollutants [122]. Thus, the presence of toluene did not affect the degradation of formaldehyde, whereas, the formaldehyde presence decreased the toluene deficiency. Jo and Kim developed N-TiO$_2$ by calcination of TiO$_2$ nanoparticles with organic nitrogen compounds (urea, guanidine hydrochloride and guanidine carbonate) as a nitrogen source, applied to the degradation of indoor level volatile organic compounds (VOCs) such as benzene, toluene, ethylbenzene, m, p-xylene and o-xylene in the presence of visible light irradiation. For all VOCs, the N-TiO$_2$ exhibited higher degradation efficiency than the unmodified TiO$_2$, whereas the degradation efficiency depends highly on the stream flow rate, hydraulic diameter and relative humidity [123]. Similarly, He et al. synthesized N-TiO$_2$ nanoparticles with anatase-brookite mixed-phase TiO$_2$ by solvothermal method using different nitrogen sources (ammonia, hydrazine hydrate or ammonium nitrate). N-TiO$_2$ prepared with hydrazine hydrate as precursor showed higher photocatalytic activity in degradation of gaseous benzene under UV light irradiation and the degradation efficiency was not changed after 15 experiment cycles [124]. Priya and Philip prepared N-TiO$_2$ and evaluated its catalytic efficiency by degradation of VOCs (methanol, acetone, dichloromethane (DCM), benzene and toluene) present in pharmaceutical wastewater under visible and solar light irradiation. The degradation rate followed an order of benzene > toluene > DCM > methanol > acetone and showed faster degradation rate under solar light irradiation [125]. Khan et al. prepared N-TiO$_2$ by co-precipitation of tri-thiocyanuric acid (TCA) with Degussa P25 TiO$_2$ followed by calcination under N$_2$ atmosphere (550 °C, 4 h). Results showed both the interstitial position of nitrogen and nitrogen substitutional doping on the oxygen site into the TiO$_2$ lattice. N-doping improved the visible-light absorption and enhanced the charge carrier's separation/transfer efficiency by capturing the holes by reduced titanium ions and showed higher photocatalytic activity in degradation of NOx under UV and visible light irradiation [63]. Recently, TiO$_2$ and N-TiO$_2$ were derived by combustion/calcination of metal organic frameworks (MOFs). Zhao et al. prepared N-TiO$_2$ with anatase-rutile phase by calcining the titanium metal organic frameworks (MIL-125 (Ti)) and melamine mixture at different temperatures in air. Results revealed that N doping is a substitutional one and

replaced the O atoms in the TiO$_2$ lattice, and the N-TiO$_2$ synthesized at 500 °C showed higher visible light photocatalytic activity than the N-TiO$_2$ synthesized at other temperature and Degussa P-25 TiO$_2$ in degradation of gaseous benzene [126]. Similarly, various research studies are available on N-TiO$_2$ that show the importance of N-TiO$_2$ and their significant visible light photocatalytic activities towards degradation of pollutants in the aqueous and gaseous phase (Table 2).

Table 2. Photocatalytic degradation of water and gaseous pollutants using N-TiO$_2$ materials.

Catalyst	Synthesis Method	Nitrogen Source	Doping Mechanism	Pollutants	Process Condition	Degradation Efficiency	Ref.
N-TiO$_2$ Thin Film TiO$_{2-x}$N$_x$	Pulsed Laser Deposition (PLD)	TiN and N$_2$/O$_2$ Mixture	Substitutional Sites of Oxygen in TiO$_2$	MB Dye	Conc.: 50 mmol/L Vol.: 150 mL, Black Light Lamp (362 nm, 50 mW/cm^2) and Fluorescent Light (540–620 nm, 120 mW/cm^2)	Same Degradation Activity Under UV (both TiO$_2$ and N-TiO$_2$ Thin Film) and N-TiO$_2$ Thin Film showed Higher Activity than the TiO$_2$ Film (visible light)	[127]
N-TiO$_2$	Sol–Gel and Calcination	NH$_3$	Ti–O–N	Trichloroethylene (TCE)	Con.: 1.8×10^{-4} mol/L, Vol.: NA, Visible Light	N-TiO$_2$ showed Higher Activity than the TiO$_2$	[128]
N-TiO$_2$	Microemulsion−hydrothermal method	Triethylamine, Urea, Thiourea, and Hydrazine hydrate	Substitutional Doping and the Doped Nitrogen are N−Ti−O and Ti−O−N.	RhB and 2,4-dichlorophenol (2,4-DCP)	Con.: 20 mg/L(RhB), and 100 mg/L (2,4-DCP), Vol.: 50 mL, 1000 W Halogen Lamp	N-TiO$_2$ with N/Ti Ratio of 2 showed Higher Activity	[88]
N-TiO$_2$	Precipitation	Ammonium Hydroxide (NH$_3$·H$_2$O)	Interstitial Site in TiO$_2$	Methyl Orange (MO)	Con.: 20 mg/L, Vol.: 80 mL, UV Lamp (8 W, 320–400 nm), Visible Light (400–650 nm)	N-TiO$_2$-400 Catalyst showed Higher Activity than the Undoped TiO$_2$ and other Concentration Loaded TiO$_2$	[129]
N-TiO$_2$	Sol Gel	NH$_4$NO$_3$/ NH$_3$·H$_2$O	Substitutional Doping	2,4-DCP	Con.: 200 mg/L, Vol.: 80 mL, 1000 W Halogen Lamp	N-TiO$_2$ Prepared at pH Value of 5.87, N/Ti Ratio of 2.0 and H$_2$O/Ti Ratio of 76 showed Higher Degradation Activity	[130]
N-TiO$_2$	Mechanochemical	NH$_4$F	-	PNP and Methyl Orange (MO)	Con.: 10 mg/L Vol.: 140 mL, UV Lamp (254 nm)	N-TiO$_2$ showed Higher Activity than the TiO$_2$	[131]
N-TiO$_2$ film	Sol Gel Method and Dip Coating	N,N,N′,N′-Tetramethylethane-1,2-Diamine (TMEDA)	Interstitial Nitrogen Doping	Resazurin Redox Dye and Stearic Acid	Con.: NA Vol.: NA, Fluorescent Lamp (9500 lx)	N-TiO$_2$ Film showed Higher Activity than the TiO$_2$	[132]

Table 2. *Cont.*

Catalyst	Synthesis Method	Nitrogen Source	Doping Mechanism	Pollutants	Process Condition	Degradation Efficiency	Ref.
N-TiO$_2$ coated glass spheres	Sol Gel Method and Dip Coating	Aqueous Ammonia Solution	-	MB and Eriochrome Black-T (EBT)	Con.: 5 mg/L Vol.: 140 mL, White Light LEDs Strip (400–800 nm), UV Emitting LEDs Strip (365–400 nm)	52% (MB, UV and Visible Light), 41% and 31% (EBT, UV and visible light)	[133]
Anatase N-TiO$_2$	Sol Gel Method	Urea, 1,6-Diaminohexane, Triethylamine	Interstitial Doping in TiO$_2$ Lattice	MB	Con.: 100 mg/L Vol.: 100 mL, 300 W Halogen Lamp	1, 6-Diaminohexane based N-TiO$_2$ showed Higher Activity	[134]
N-TiO$_2$	Ultraviolet-Assisted Thermal Synthesis	HNO$_3$	Substitutional or Interstitial	MO	Con.: 30 mg/L Vol.: NA, UV-A (254 nm), UV-B (310 nm), UV-C (365 nm) and Visible Light (470 nm), 9W Each	2.17% (visible), 26.54% (UV-A), 34.92% (UV-B), and 75.88% (UV-C)	[80]
N-TiO$_2$	Hydrothermal	Urea	Substitutional and/or Interstitial Site	Ciprofloxacin	Con.: 20 ppm Vol.: NA, 365 nm UV-A Lamps (20W)	94.29%	[90]
N-TiO$_2$ fibers	Centrifugal Spinning and Subsequent Calcination	Polyvinylpyrrolidone	–	MB	Con.: 10 ppm Vol.: 20 mL, UV and Visible Light (9W)	68.00%	[135]
N-TiO$_2$	Decomposition	Urea, Semicarbazide and N,N′-Dimethyl urea	TiO$_2$ Lattice	MB and RhB	Con.: 10 ppm (MB), 20 ppm (RhB) Vol.: 25 mL, UV and Visible Light	N-TiO$_2$ showed Higher Activity than the TiO$_2$	[117]
Gradient N-TiO$_2$	Pulsed Laser Deposition		Substitutional	Sulfamethoxazole (SMX)	Con.: 1 mg/L Vol.: 50 mL, Solar Simulator	85%	[91]
N-TiO$_2$ nanotube	Solid State Dispersion	Urea	–	MO	Con.: 3×10^{-5} mol/L, Vol.: 100 mL, Solar Light	91%	[136]
N-TiO$_2$	Wet Chemical Method	Urea	Substitutional Doping in TiO$_2$ Lattice	MB	Con.: 10 mg/L, Vol.: 10 mL, Visible Light	72%	[137]
Molecularly imprinted N-TiO$_2$	Sol–Gel Technique	NH$_4$NO$_3$	Interstitial Nitrogen Doping in TiO$_2$ Lattice	o-Phenylphenol Fungicide	Con.: 1×10^{-4} M, Vol.: 4 mL, UV Lamp	~46%	[138]
N-mixed-phase TiO2	Pyrolysis	Urea	Interstitial N Atoms in TiO$_2$ Lattice	Selective Oxidation of Cyclohexane	Con.: 1×10^{-4} M, Vol.: 4 mL, 300 W Xe Lamp	N-TiO$_2$ showed Higher Activity and Selectivity	[139]
N-TiO$_2$ and Tourmaline-nitrogen co-doped TiO$_2$	Sol–Gel	Ammonium Hydroxide	–	Bacteria, Mycobacteria, and Fungi	Con.: 10^5 to 10^7 CFU/mL, Vol.: NA, Fluorescent Lamp	Tourmaline-Nitrogen Co-Doped TiO$_2$ showed High Inactivation Efficiency	[140]

Table 2. *Cont.*

Catalyst Gaseous	Synthesis Method	Nitrogen Source	Doping Mechanism	Pollutants	Process Condition	Degradation Efficiency	Ref.
Yellow-Colored N-TiO$_2$	Spray Pyrolysis	Urea, Guanidine, or Ammonium Fluoride	–	Acetaldehyde and TCE	Con.: 930 ppm, Vol.: NA, 150 W Xe Lamp	N-TiO$_2$ showed Higher Activity in Acetaldehyde and TCE Degradation	[121]
Ultrastable N-TiO$_2$	Sol–Gel	Urea	Interstitial N Atoms	Acetaldehyde	Con.: 1000 ppm, Flow Rate: 10 mL/min Vol.: NA, 400 W Xe Lamp	25%	[141]
N-TiO$_2$	Solvothermal Method	Ammonia (ANT), Hydrazine Hydrate (HNT), Ammonium Nitrate (NNT)		Benzene	Con.: 2 μL (180 mg/m^3), Vol.: NA, 250 WUV Lamp (Hg)	91%	[124]
TiO$_{2-x}$N$_y$ Coupled with Long-Afterglow Phosphors	Hydrothermal	Hexamethylenetetramine	–	Acetaldehyde	Con.: 10 Mass %, Vol.: NA, 10 W Black Light	60 Mass % CaAl$_2$O$_4$:(Eu, Nd)/40 Mass % TiO$_{2-x}$N$_y$ showed Higher Activity	[142]

9.2. Water Splitting (H$_2$ Production)

In order to fulfill the increasing energy demands and eradicate environmental problems, the generation of energy from renewable resources is receiving significant attention. Splitting of water into hydrogen (H$_2$) and oxygen (O$_2$) is one of the sustainable processes for the production of renewable energy. For higher H$_2$ production efficiency, the CB and VB position of semiconductors must be higher than the H$_2$ (H$^+$/H$_2$, 0 V) and O$_2$ (O$_2$/H$_2$O, 1.23 V) evolution potentials. Furthermore, the water splitting reactions are majorly performed in the pure water medium and addition of the sacrificial agents, and also photoreforming of wastewater (simultaneous production of H$_2$ and degradation of pollutants). Various semiconductor nanomaterials have been utilized for the H$_2$ production reaction, in which N-TiO$_2$ is one of the catalytic systems effectively used for this purpose under the irradiation of visible light [15,143–147].

Babu et al. developed a rice-grain-like N-TiO$_2$ nanostructure morphology using combined sol–gel and electrospinning followed by an annealing process. N doping did not change the morphology, crystallinity and d-spacing of the TiO$_2$ fibers. No variation in the d-spacing of the nanostructure's anatase (101) plane shows that the N has been doped into the TiO$_2$ lattice (substitutional N-doping) without altering the unit cell dimension, which was confirmed by XPS analysis. N-TiO$_2$ (28 μmol/h) exhibited enhanced water splitting efficiency compared to TiO$_2$ fibers (2 μmol/h). Likewise, N-TiO$_2$ fibers showed higher methylene blue dye degradation efficiency [148]. Similarly, N-TiO$_2$ was developed by the controlled oxidation of titanium nitride at different temperatures (350 °C, 400 °C and 450 °C) and that the color changes from black to yellow confirmed the formation of N-TiO$_2$. The nitrogen doping occurred on the TiO$_2$ lattice showed shifting of binding energy values of Ti 2p to higher values in the XPS. The N-TiO$_2$ sample (N-TiO$_2$-450) showed the higher H$_2$-evolution potential than the Degussa P-25 TiO$_2$ in a Na$_2$S-Na$_2$SO$_3$ sacrificial system under UV-Vis light irradiation [149]. Wang et al. prepared N-doped TiO$_2$ on quartz glass with preferred (112) and (211) facet orientation by RF magnetron sputtering method using

a mixture of N_2, O_2 and Ar gas. XPS analysis indicated that the binding energy value at 396.5 eV validated the substitutional integration of N into the TiO_2 film. Furthermore, by increasing the N_2 gas flow rate, the growth of preferred (211) facet orientation is increased, which leads to higher surface energies of anatase facets ((112) and (211)) than the (101) facet of anatase TiO_2. The huge percentage of exposed facets, especially (211) facets, showed higher photocatalytic water splitting efficiency (4500 µmol H_2 h^{-1} m^{-2}) than the undoped TiO_2 film. In addition, the high surface energy (211) facets would destabilize the O 2p states on the surface where the water molecules are easily absorbed and dissociated, which leads to higher water splitting efficiency [150]. Similarly, Fakhouri et al. developed pure and N-TiO_2 thin films through RF reactive magnetron sputtering method, and observed both substitutional and interstitial N doping onto TiO_2 thin films. Photocatalytic ability was evaluated by degradation of N-methyl-2-pyrrolidone (NMP) and water splitting reaction under light irradiation (both UV and visible). Both the film morphology and N doping sites have significant effect on the photocatalytic ability. The increase in the interstitial N-doping sites enhanced the photocatalytic activity; whereas increases in the substitutional N-doping sites decrease the activity under UV light irradiation but not under visible light. This could be attributed to the recombination of photo-generated charge carriers when the films have more substitutional nitrogen and decreased activity under UV light. Furthermore, TiO_2 film with dominant interstitial N doping sites progress photocatalytic activity, due to the separation of photoproduced charge separation on the porous films having higher surface area than the anticipated surface [151]. Similarly, Sun et al. prepared surface heterojunction N-TiO_2 nanobelt structures with co-exposed (001) and (101) facets and showed diverse transmission properties and reactivity for photogenerated charge carriers and enhanced photocatalytic ability. N-TiO_2 nanobelts form the surface heterojunction that induces an electrostatic force, in which the electrons in the (001) facet are immediately attracted to the (101) facet, transferred to the surface (active reaction sites) and combine with H^+ and form H_2. Water splitting reaction revealed N-TiO_2 nanobelts with co-exposed (001) and (101) facets showed higher H_2 production (670 µmol h^{-1} g^{-1}) rate than the other N-TiO_2 nanobelts with a single facet exposed [152]. Recently, Esmat et al. developed an oxygen vacancy (Vo)-bearing N-doped anatase TiO_2 through the calcination of layered titanate nanosheets comprising N, N-dimethylformamide (DMF), an organic N source, in air. XPS analysis demonstrated that N 1s shows two peaks at 402.2 eV and 400.1 eV, corresponded to the nitrogen in the adsorbed DMF and interstitial doping of nitrogen in TiO_2 lattices validating the presence of Ti−O−N bond and the concomitant creation of Vo. N doping and the formation of Vo significantly enhanced the light absorption of TiO_2 (up to 500 nm). Furthermore, the introduction of Vo donates the electrons in TiO_2, facilitating the photogenerated charge carrier separation and transfer which leads to more enhanced water splitting efficiency (1035 µmol h^{-1} g^{-1}) than the undoped TiO_2 (~300 µmol h^{-1} g^{-1}) [153]. Similarly, various research studies are available on N-TiO_2 photocatalyst for hydrogen production application, which are summarized in Table 3.

Table 3. Photocatalytic splitting of water into H_2 and O_2 using N-TiO_2 materials.

Catalyst	Synthesis Method	Nitrogen Source	Doping Mechanism	Medium Used for Water Splitting	Process Condition	H_2O Splitting Efficiency	Ref.
N-TiO_2	Solid State and Sol Gel	Urea and NH_4NO_3	Surface Doping	Aqueous Solution of Formic Acid	25 W Black-Light Compact Fluorescent UVA Lamps or 4 × 15 W Visible Compact Fluorescent Lamps	24.5 µmol H_2 (TiO_2, UVA), 3.2 µmol (TiO_2, visible), 72.7 µmol H_2 (N-TiO_2, UVA)	[154]

Table 3. *Cont.*

Catalyst	Synthesis Method	Nitrogen Source	Doping Mechanism	Medium Used for Water Splitting	Process Condition	H_2O Splitting Efficiency	Ref.
N-TiO$_2$	Microwave-Assisted Hydrothermal	Urea	Interstitial N Doping	Aqueous Solution of Methanol	Vol.: 100 mL (vol. ratio of MeOH:H$_2$O = 1:5), 500 W Halogen and 400 W Medium Pressure Halide Lamp	4386 µmol/g/h (UV), 185 µmol/g/h (visible)	[155]
N-TiO$_2$ film	RF Reactive Magnetron Sputtering	Mixture of N$_2$, O$_2$ and Ar	TiO$_2$ Lattice	Aqueous Solution of Methanol	Vol.: 100 mL (CH$_3$OH: H$_2$O = 1:10 *v/v*), 300 W Xe Lamp	601 µmol/g/h	[156]
N-doped anatase-rutile TiO$_2$	Potentiostatic Rapid Breakdown Anodization Technique	NH$_3$	Interstitial Nitrogen and Surface Adsorbed N Atoms	Aqueous Solution of Ethanol	Vol.: 50 mL, Solar Simulator (145 mW/cm^2)	~30 mmol/h/g	[157]
N-doped multiphase TiO$_2$ (e.g., anatase (69%)/brookite (17%)/rutile (14%))	Hydrothermal	Urea	Substitutional N Doping	Water	Vol.: 50 mL, Solar Light (100,000 L)	10,500 µmol/h/g, P25 (1700 µmol/h/g)	[158]
N-doped mesoporous TiO$_2$	Simple Solvent Evaporation Induced Self-Assembly	N-Containing Ionic Liquid	Substitutional N Doping	Aqueous Solution of Methanol	Vol.: 155 mL (25.8 vol%), 450 W Xe Lamp	39.1 µmol/g/h	[159]
N-TiO$_2$	Single-Step Hydrolysis Method	Pyridine	Interstitially N Doping	Aqueous Solution of Methanol	Solar Light	3500 µ mol/h/g	[160]
N-TiO$_2$ nanotube	Solid State Dispersion	Urea	Substitutional N Doping	H$_2$O + Glycerol	Vol.: 50 mL (5 vol%), Solar Light (110,000 to 140,000 l×)	19,848 µmol/h/g	[136]

10. Stability, Recovery and Reusability of N-TiO$_2$ Photocatalyst

The stability of photocatalyst is one of the important factors for up-scaling the developed photocatalytic systems for field level applications. Generally, the stability of the photocatalyst was determined by performing the catalytic recycle experiment. Initially the catalytic materials recovered from the reaction mixture by either centrifugation, filtration, or both processes, are then subjected to various chemical and physical methods for purifying/cleaning the catalytic materials and reused for the same catalytic reaction. For example, Zeng et al. developed a N-TiO$_2$ by combination of precipitation with thermal decomposition method using urea, ammonium chloride and ammonium nitrate as nitrogen sources, for the degradation of flumequine (FLU) antibiotic under visible light irradiation. The N-TiO$_2$ prepared with ammonium nitrate showed higher photocatalytic activity than the pure TiO$_2$. The stability and reusability of the N-TiO$_2$ was evaluated by degradation of FLU in four recycling experiments. After the first cycle, the catalyst was recovered by centrifugation and washed three times with ultrapure water, then the fresh FLU solution

was added and the degradation experiment was performed. The same procedure was repeated for three cycles (Figure 16). The results demonstrated that after the first cycle the FLU was completely removed and afterwards the FLU removal efficiency remained at 91.8% after four cycles of experiment. The degradation efficiency is slightly affected during four consecutive cycles which may be due to the loss of materials during the washing process, and also indicates that the N-TiO$_2$ prepared with ammonium nitrate showed good stability [119].
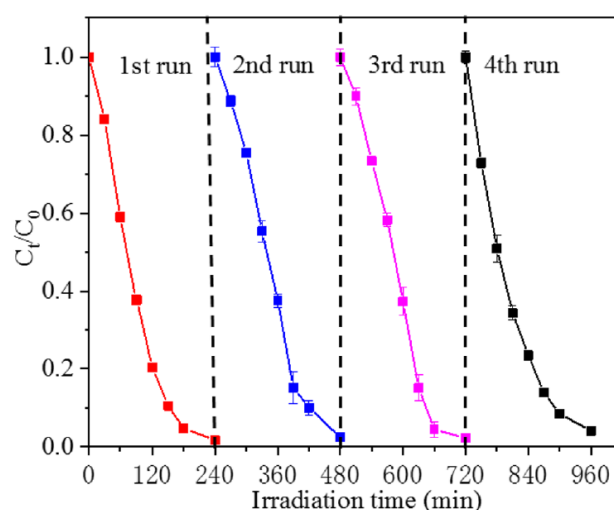
Figure 16. The stability of N-TiO$_2$ (prepared with ammonium nitrate) for FLU degradation under visible light irradiation. Reprinted with permission from [119].

Similarly, Mirzaei et al. (2021) prepared a gradient nitrogen-doped TiO$_2$ (g-N-TiO$_2$) by PLD method for the removal of sulfamethoxazole (SMX) antibiotic in water in the presence of simulated solar light irradiation. The g-N-TiO$_2$ showed superior photocatalytic activity in degradation of SMX compared to pure TiO$_2$ and N-TiO$_2$. The stability and reusability of the materials was evaluated by performing three consecutive runs, revealing that maximum ~12% loss in the SMX removal was obtained and the photocatalyst was very stable (Figure 17) [91].

From this catalytic recovery process, it is understood that there is a material loss during either centrifugation, filtration, or both; therefore, decrease in the photocatalytic catalytic activity was observed after the second or third cycles of experiment. Therefore, recently, the immobilization of catalytic materials on the magnetic support have been performed which helps to easily collect and separate the materials by applying an external magnetic field. Zangeneh et al. prepared visible light active magnetic N-TiO$_2$/ZnFe$_2$O$_4$ and CN-co-doped TiO$_2$/ZnFe$_2$O$_4$ nanocomposite materials by sol–gel–hydrothermal method using urea and L-asparagine as nitrogen source. The photocatalytic activity evaluation results demonstrated that 2 wt.% of L-asparagine derived CN–TiO$_2$/ZnFe$_2$O$_4$ (97%) showed superior visible light photocatalytic activity than the CN–TiO$_2$ (90.5%), N–TiO$_2$/ZnFe$_2$O$_4$ (70%), N–TiO$_2$ (53%) and pure TiO$_2$ (30%) in degradation of direct red 16 (DR16) dye. After the first cycle of the experiment, the photocatalyst was recovered by the external magnetic field, washed with distilled water, irradiated under visible light (3 h) for degradation of adsorbed pollutants and dried (100 °C). Thereafter, the degradation experiment was repeated for six cycles, up to four cycles no loss in the photoactivity of the materials was noted and then 7% loss in degradation efficiency was observed. The results revealed that the photocatalyst can be completely recovered by applying an external magnetic field, which was confirmed by vibrating sample magnetometer (VSM) analysis results [161].
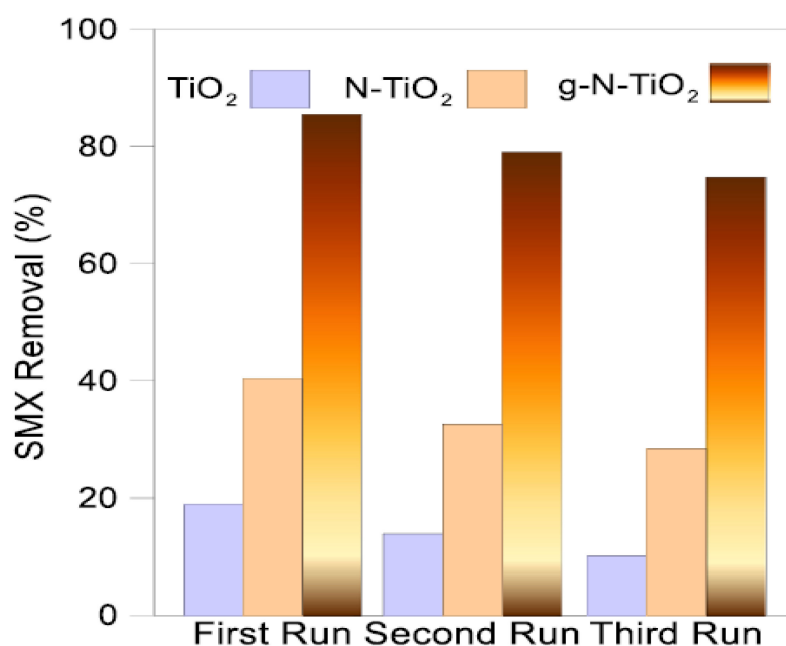
Figure 17. Recycling test of SMX degradation using TiO_2, $N-TiO_2$ and $g-N-TiO_2$ photocatalysts. Reprinted with permission from [91].

11. Opportunity, Challenges and Future Requirement/Prospects

TiO_2 is a potential semiconducting nanomaterial for the environmental remediation, energy production, sensors, solar cells, self-cleaning of tiles, glass and windows and antifogging applications, etc., and the same has also been demonstrated at commercial scale and well-documented. Furthermore, clean solar energy can be harnessed for development of sustainable and economically viable effluent treatment technologies. Therefore, N-doped TiO_2 is one of the efficient visible light responsive photocatalysts for harvesting solar light and utilizing it for various applications. As described above, various literature evidences revealed the various synthesis methodologies for preparation of efficient $N-TiO_2$ and evaluated its physicochemical and electronic properties. However, challenges still remain with respect to the understanding of nitrogen doping mechanisms, influence of nitrogen concentration on its position in the TiO_2 lattice, photogenerated charge carrier dynamics, influence of heating on phase transformation, reactive radical's generation and their concentration on catalytic efficiency. Therefore, the following research gaps/opportunities are available and need to be considered to fulfil the future direction of development of effective N-doped TiO_2 photocatalytic systems for the environmental remediation, energy harvesting and production applications.

(a) The defects in TiO_2, electronic structure of disordered TiO_2, physicochemical properties and their influence on the catalytic efficiency needs to be investigated.

(b) Each methodology involves different operational parameters and uses different nitrogen sources which limit the synthesis optimizing N doping and also upgradation of large-scale synthesis of efficient $N-TiO_2$ for practical implementation. Therefore, there is an urgent need for an optimized synthesized methodology and nitrogen sources for preparation of $N-TiO_2$ and this could be a promising photoresponsive nanomaterials research.

(c) The stability of $N-TiO_2$ is still questionable, thus the co-doping of $N-TiO_2$ with other metals, non-metals and semiconductors could improve its stability and reusability, thus boosting the practical applicability of the materials. However, the study of the practical degradation ability of the $N-TiO_2$ systems in realistic wastewater is needed.

(d) The recovery and reusability of $N-TiO_2$ could be improved by integrating/supporting $N-TiO_2$ on magnetic supports. However, there is still a decrease in photocatalytic effi-

ciency due to the loss of materials after several cycles and also the energy requirement for post-treatment of recovered catalyst is still on the high side. Therefore, the immobilization of photocatalytic materials on various solid supports followed by fabrication of different geometry of reactors have been performed, and the catalytic materials are easily recovered after the catalytic reaction and reused for multiple cycles of experiments while retaining photocatalytic efficiency. However, the upscaling of the process for real scale application depends upon the various operational parameters (e.g., coating techniques, reproducibility in coating thickness, etc.). Therefore, there is an opportunity to optimize the various operational parameters for designing effective immobilized photocatalytic reactor systems.

(e) The N doping/incorporation into TiO_2 is still debatable and it depends upon the sources of nitrogen and the synthesis methodologies adopted. Furthermore, controlling the N doping concentration in the TiO_2 lattice is essential for efficient catalytic efficiency. Therefore, the characterization of N-TiO_2 using combined analytical techniques (e.g., transient optical spectroscopy) along with theoretical study is needed to control the doping concentration and create awareness of the structural features of the N-TiO_2.

(f) Theoretical analysis and computational modeling of the experimental data is needed that offers clear representation on the required nitrogen source type, synthesis methodology for development of durable N-doped TiO_2, structure, doping mechanism and the catalytic efficiency of N-TiO_2.

12. Summary and Conclusions

N-TiO_2 is one of the efficient non-metal-doped visible light active photocatalysts for the removal of environmental pollutants and renewable energy production. Nitrogen doping enhances visible light absorption through narrowing the bandgap energy and improves the photoproduced charge separation and transfer efficiency. In this review, we summarize the various synthesis methodologies adopted and nitrogen sources used for preparation of N-TiO_2 and also their influence on the catalytic efficiency. Further, the possible mechanisms for N doping, changes in the properties and their visible-light catalytic applications in pollutants degradation and water splitting reactions are discussed. It could be understood that each method is unique in their approach for preparation of N-TiO_2 with excellent photocatalytic efficiency. The modifications in the reaction operational parameters and the co-doping offers excellent structural, textural and electronic properties to N-doped TiO_2, which leads to enhanced visible-light photocatalytic efficiency. In addition, the above-mentioned research gaps need to be focused on for the development of efficient renewable solar-energy-based photocatalytic systems. Thus, N-TiO_2 could be considered as an efficient counterpart to noble metal and other metal-doped TiO_2 systems.

References

1. Fujishima:, A.; Honda, K. Electrochemical Photolysis of Water at a Semiconductor Electrode. *Nature* **1972**, *238*, 37. [CrossRef] [PubMed]
2. Tayade, R.J.; Kulkarni, R.G.; Jasra, R.V. Photocatalytic Degradation of Aqueous Nitrobenzene by Nanocrystalline TiO$_2$. *Ind. Eng. Chem. Res.* **2006**, *45*, 922–927. [CrossRef]
3. Tayade, R.J.; Surolia, P.K.; Kulkarni, R.G.; Jasra, R.V. Photocatalytic degradation of dyes and organic contaminants in water using nanocrystalline anatase and rutile TiO$_2$. *Sci. Technol. Adv. Mater.* **2007**, *8*, 455–462. [CrossRef]
4. Natarajan, K.; Natarajan, T.S.; Kureshy, R.I.; Bajaj, H.C.; Jo, W.K.; Tayade, R.J. Photocatalytic H$_2$ Production using Semiconductor Nanomaterials via Water Splitting—An Overview. In *Advanced Materials Research*; Al-Ahmed, A., Hossain, M.K., Afzaal, M., Bahaidarah, H.M., Eds.; Trans Tech Publications, Ltd.: Stafa-Zurich, Switzerland, 2015; Volume 1116, pp. 130–156.
5. Schneider, J.; Matsuoka, M.; Takeuchi, M.; Zhang, J.; Horiuchi, Y.; Anpo, M.; Bahnemann, D.W. Understanding TiO$_2$ Photocatalysis: Mechanisms and Materials. *Chem. Rev.* **2014**, *114*, 9919–9986. [CrossRef] [PubMed]
6. Humayun, M.; Raziq, F.; Khan, A.; Luo, W. Modification strategies of TiO$_2$ for potential applications in photocatalysis: A critical review. *Green Chem. Lett. Rev.* **2018**, *11*, 86–102. [CrossRef]
7. Ali, I.; Suhail, M.; Alothman, Z.A.; Alwarthan, A. Recent advances in syntheses, properties and applications of TiO$_2$ nanostructures. *RSC Adv.* **2018**, *8*, 30125–30147. [CrossRef]
8. Natarajan, T.S.; Tayade, R.J. Photocatalysis: Present, past and future. In *Inorganic Pollutants in Wastewater: Method of Analysis, Removal and Treatment*; Inamuddin, Mohammad, A., Asiri, A.M., Eds.; Materials Research Forum LLC: Millersville, PA, USA, 2017; Volume 16, pp. 1–63.
9. Asahi, R.; Morikawa, T.; Irie, H.; Ohwaki, T. Nitrogen-Doped Titanium Dioxide as Visible-Light-Sensitive Photocatalyst: Designs, Developments, and Prospects. *Chem. Rev.* **2014**, *114*, 9824–9852. [CrossRef]
10. Natarajan, S.; Bajaj, H.C.; Tayade, R.J. Recent advances based on the synergetic effect of adsorption for removal of dyes from waste water using photocatalytic process. *J. Environ. Sci.* **2018**, *65*, 201–222. [CrossRef]
11. Tayade, R.J.; Kulkarni, R.G.; Jasra, R.V. Transition metal ion impregnated mesoporous TiO$_2$ for photocatalytic degradation of organic contaminants in water. *Ind. Eng. Chem. Res.* **2006**, *45*, 5231–5238. [CrossRef]
12. Natarajan, T.S.; Natarajan, K.; Bajaj, H.C.; Tayade, R.J. Enhanced photocatalytic activity of bismuth-doped TiO$_2$ nanotubes under direct sunlight irradiation for degradation of Rhodamine B dye. *J. Nanoparticle Res.* **2013**, *15*, 1–18. [CrossRef]
13. Devi, L.G.; Kavitha, R. A review on non metal ion doped titania for the photocatalytic degradation of organic pollutants under UV/solar light: Role of photogenerated charge carrier dynamics in enhancing the activity. *Appl. Catal. B Environ.* **2013**, *140–141*, 559–587. [CrossRef]
14. Ansari, S.A.; Khan, M.M.; Ansaric, M.O.; Cho, M.H. Nitrogen-doped titanium dioxide (N-doped TiO$_2$) for visible light photocatalysis. *New J. Chem.* **2016**, *40*, 3000–3009. [CrossRef]
15. Bakar, S.A.; Ribeiro, C. Nitrogen-doped titanium dioxide: An overview of material design and dimensionality effect over modern applications. *J. Photochem. Photobiol. C Photochem. Rev.* **2016**, *27*, 1–29. [CrossRef]
16. Varma, K.S.; Tayade, R.J.; Shah, K.J.; Joshi, P.A.; Shukla, A.D.; Gandhi, V.G. Photocatalytic degradation of pharmaceutical and pesticide compounds (PPCs) using doped TiO$_2$ nanomaterials: A review. *Water Energy Nexus* **2020**, *3*, 46–61. [CrossRef]
17. Tayade, R.J.; Kulkarni, R.G.; Jasra, R.V. Enhanced Photocatalytic Activity of TiO$_2$-Coated NaY and HY Zeolites for the Degradation of Methylene Blue in Water. *Ind. Eng. Chem. Res.* **2007**, *46*, 369–376. [CrossRef]
18. Palanivelu, K.; Im, J.S.; Lee, Y.-S. Carbon Doping of TiO$_2$ for Visible Light Photo Catalysis—A review. *Carbon Sci.* **2007**, *8*, 214–224. [CrossRef]
19. Tayade, R.J.; Surolia, P.K.; Lazar, M.A.; Jasra, R.V. Enhanced Photocatalytic Activity by Silver Metal Ion Exchanged NaY Zeolite Photocatalysts for the Degradation of Organic Contaminants and Dyes in Aqueous Medium. *Ind. Eng. Chem. Res.* **2008**, *47*, 7545–7551. [CrossRef]
20. Jo, W.-K.; Won, Y.; Hwang, I.; Tayade, R.J. Enhanced Photocatalytic Degradation of Aqueous Nitrobenzene Using Graphitic Carbon−TiO$_2$ Composites. *Ind. Eng. Chem. Res.* **2014**, *53*, 3455–3461. [CrossRef]
21. Mogilevsky, G.; Hartman, O.; Emmons, E.D.; Balboa, A.; DeCoste, J.B.; Schindler, B.J.; Iordanov, I.; Karwacki, C.J. Bottom-Up Synthesis of Anatase Nanoparticles with Graphene Domains. *ACS Appl. Mater. Interfaces* **2014**, *6*, 10638–10648. [CrossRef]
22. Natarajan, T.S.; Bajaj, H.C.; Tayade, R.J. Palmyra tuber peel derived activated carbon and anatase TiO$_2$ nanotube based nanocomposites with enhanced photocatalytic performance in rhodamine 6G dye degradation. *Process. Saf. Environ. Prot.* **2016**, *104*, 346–357. [CrossRef]
23. Giovannetti, R.; Rommozzi, E.; Zannotti, M.; D'Amato, C.A. Recent Advances in Graphene Based TiO$_2$ Nanocomposites (GTiO$_2$Ns) for Photocatalytic Degradation of Synthetic Dyes. *Catalysts* **2017**, *7*, 305. [CrossRef]
24. Natarajan, T.S.; Lee, J.Y.; Bajaj, H.C.; Jo, W.K.; Tayade, R.J. Synthesis of multiwall carbon nanotubes/TiO$_2$ nanotube composites with enhanced photocatalytic decomposition efficiency. *Catal. Today* **2017**, *282*, 13–23. [CrossRef]
25. Thomas, M.; Natarajan, T.S. TiO$_2$-High Surface Area Materials Based Composite Photocatalytic Nanomaterials for Degradation of Pollutants: A Review. In *Photocatalytic Nanomaterials for Environmental Applications*; Tayade, R.J., Gandhi, V., Eds.; Materials Research Forum LLC: Millersville, PA, USA, 2018; Volume 27, pp. 48–96.
26. Hua, L.; Yin, Z.; Cao, S. Recent Advances in Synthesis and Applications of Carbon-Doped TiO$_2$ Nanomaterials. *Catalysts* **2020**, *10*, 1431. [CrossRef]

27. Yalçın, Y.; Kılıç, M.; Çınar, Z. The Role of Non-Metal Doping in TiO$_2$ Photocatalysis. *J. Adv. Oxid. Technol.* **2016**, *13*, 281–296. [CrossRef]
28. Sato, S. Photocatalytic activity of NO$_x$-doped TiO$_2$ in the visible light region. *Chem. Phys. Lett.* **1986**, *123*, 126–128. [CrossRef]
29. Asahi, R.; Morikawa, T.; Ohwaki, T.; Aoki, K.; Taga, Y. Visible-Light Photocatalysis in Nitrogen-Doped Titanium Oxides. *Science* **2001**, *294*, 269–271. [CrossRef]
30. Fox, M.A.; Dulay, M.T. Heterogeneous photocatalysis. *Chem. Rev.* **1993**, *93*, 341–357. [CrossRef]
31. Acharya, R.; Naik, B.; Parida, K. Cr(VI) remediation from aqueous environment through modified-TiO$_2$-mediated photocatalytic reduction. *Beilstein J. Nanotechnol.* **2018**, *9*, 1448–1470. [CrossRef]
32. Gomes, J.; Lincho, J.; Domingues, E.; Quinta-Ferreira, R.M.; Martins, R.C. N–TiO$_2$ Photocatalysts: A Review of Their Characteristics and Capacity for Emerging Contaminants Removal. *Water* **2019**, *11*, 373. [CrossRef]
33. Ismael, M. A review and recent advances in solar-to-hydrogen energy conversion based on photocatalytic water splitting over doped-TiO$_2$ nanoparticles. *Sol. Energy* **2020**, *211*, 522–546. [CrossRef]
34. Rivas, J.; Solis, R.R.; Gimeno, O.; Sagasti, J. Photocatalytic elimination of aqueous 2-methyl-4-chlorophenoxyacetic acid in the presence of commercial and nitrogen-doped TiO$_2$. *Int. J. Environ. Sci. Technol.* **2015**, *12*, 513–526. [CrossRef]
35. Solís, R.R.; Rivas, F.J.; Gimeno, O.; Pérez-Bote, J.L. Photocatalytic ozonation of pyridine-based herbicides by N-doped titania. *J. Chem. Technol. Biotechnol.* **2016**, *91*, 1998–2008. [CrossRef]
36. Solís, R.R.; Rivas, F.J.; Martínez-Piernas, A.; Agüera, A. Ozonation, photocatalysis and photocatalytic ozonation of diuron. Intermediates identification. *Chem. Eng. J.* **2016**, *292*, 72–81. [CrossRef]
37. Avisar, D.; Horovitz, I.; Lozzi, L.; Ruggieri, F.; Baker, M.; Abel, M.-L.; Mamane, H. Impact of water quality on removal of carbamazepine in natural waters by N-doped TiO$_2$ photo-catalytic thin film surfaces. *J. Hazard. Mater.* **2013**, *244–245*, 463–471. [CrossRef]
38. Caratto, V.; Setti, L.; Campodonico, S.; Carnasciali, M.M.; Botter, R.; Ferretti, M. Synthesis and characterization of nitrogen-doped TiO$_2$ nanoparticles prepared by sol–gel method. *J. Sol. Gel. Sci. Technol.* **2012**, *63*, 16–22. [CrossRef]
39. Pan, J.H.; Han, G.; Zhou, R.; Zhao, X.S. Hierarchical N-doped TiO$_2$ hollow microspheres consisting of nanothorns with exposed anatase {101} facets. *Chem. Commun.* **2011**, *47*, 6942–6944. [CrossRef]
40. Chainarong, S.; Sikong, L.; Pavasupree, S.; Niyomwas, S. Synthesis and Characterization of Nitrogen-doped TiO$_2$ Nanomaterials for Photocatalytic Activities under Visible Light. *Energy Procedia* **2011**, *9*, 418–427. [CrossRef]
41. Yin, S.; Zhang, Q.; Saito, F.; Sato, T. Preparation of visible light-activated titania photocatalyst by mechanochemical method. *Chem. Lett.* **2003**, *32*, 358–359. [CrossRef]
42. Yin, S.; Yamaki, H.; Komatsu, M.; Zhang, Q.; Wang, J.; Tang, Q.; Saito, F.; Sato, T. Preparation of nitrogen-doped titania with high visible light induced photocatalytic activity by mechanochemical reaction of titania and hexamethylenetetramine. *J. Mater. Chem.* **2003**, *13*, 2996–3001. [CrossRef]
43. Techitdheera, W.; Rattanarak, J.; Mekprasart, W.; Pecharapa, W. Influence of milling time, NH$_3$ additive and annealing temperature on physical properties of modified commercial TiO$_2$ powders via ball milling process. *Energy Procedia* **2014**, *56*, 667–672. [CrossRef]
44. Kassim, K.; Hamali, M.A.; Yamin, B. A new alternative synthesis of salicylaldazine via microwave irradiation method. *J. Chem.* **2019**, *2019*, 9546373. [CrossRef]
45. Eskicioglu, C.; Terzian, N.; Kennedy, K.J.; Droste, R.L.; Hamoda, M. Athermal microwave effects for enhancing digestibility of waste activated sludge. *Water Res.* **2007**, *41*, 2457–2466. [CrossRef]
46. Kadam, A.N.; Dhabbe, R.S.; Kokate, M.R.; Gaikwad, Y.B.; Garadkar, K.M. Preparation of N doped TiO$_2$ via microwave-assisted method and its photocatalytic activity for degradation of Malathion. *Spectrochim. Acta Part A Mol. Biomol. Spectrosc.* **2014**, *133*, 669–676. [CrossRef]
47. Azami, M.S.; Nawawi, W.I.; Jawad, A.H.; Ishak, M.A.M.; Ismail, K. N-doped TiO$_2$ Synthesised via Microwave Induced Photocatalytic on RR4 Dye Removal under LED Light Irradiation. *Sains Malays.* **2017**, *46*, 1309–1316. [CrossRef]
48. Lin, Y.-H.; Weng, C.-H.; Srivastav, A.L.; Lin, Y.-T.; Tzeng, J.-H. Facile Synthesis and Characterization of N-Doped TiO$_2$ Photocatalyst and Its Visible-Light Activity for Photo-Oxidation of Ethylene. *J. Nanomater.* **2015**, *2015*, 807394. [CrossRef]
49. Makropoulou, T.; Panagiotopoulou, P.; Venieri, D. N-doped TiO$_2$ photocatalysts for bacterial inactivation in water. *J. Chem. Technol. Biotechnol.* **2018**, *93*, 2518–2526. [CrossRef]
50. Irie, H.; Washizuka, S.; Watanabe, Y.; Kako, T.; Hashimoto, K. Photoinduced hydrophilic and electrochemical properties of nitrogen-doped TiO$_2$ films. *J. Electrochem. Soc.* **2005**, *152*, E351. [CrossRef]
51. Kitano, M.; Funatsu, K.; Matsuoka, M.; Ueshima, M.; Anpo, M. Preparation of nitrogen-substituted TiO$_2$ thin film photocatalysts by the radio frequency magnetron sputtering deposition method and their photocatalytic reactivity under visible light irradiation. *J. Phys. Chem. B* **2006**, *110*, 25266–25272. [CrossRef]
52. Obata, K.; Irie, H.; Hashimoto, K. Enhanced photocatalytic activities of Ta, N co-doped TiO$_2$ thin films under visible light. *Chem. Phys.* **2007**, *339*, 124–132. [CrossRef]
53. Dobromir, M.; Manole, A.V.; Nica, V.; Apetrei, R.; Neagu, M.; Luca, D. Analyzing the Development of N-Doped TiO$_2$ Thin Films Deposited by RF Magnetron Sputtering. *Sens. Lett.* **2013**, *11*, 675–678. [CrossRef]
54. Chan, M.-H.; Lu, F.-H. Characterization of N-doped TiO$_2$ films prepared by reactive sputtering using air/Ar mixtures. *Thin Solid Film.* **2009**, *518*, 1369–1372. [CrossRef]

55.	Chen, X.; Ma, E.; Liu, G.; Yin, M. Excited-state dynamics of Er^{3+} in Gd$_2$O$_3$ nanocrystals. *J. Phys. Chem. C* **2007**, *111*, 9638–9643. [CrossRef]

56.	Tang, J.; Zou, Z.; Ye, J. Photophysical and photocatalytic properties of AgInW$_2$O$_8$. *J. Phys. Chem. B* **2003**, *107*, 14265–14269. [CrossRef]

57.	Matsubara, K.; Danno, M.; Inoue, M.; Honda, Y.; Abe, T. Characterization of nitrogen-doped TiO$_2$ powder prepared by newly developed plasma-treatment system. *Chem. Eng. J.* **2012**, *181–182*, 754–760. [CrossRef]

58.	Yamada, K.; Nakamura, H.; Matsushima, S.; Yamane, H.; Haishi, T.; Ohira, K.; Kumada, K. Preparation of N-doped TiO$_2$ particles by plasma surface modification. *Comptes Rendus Chim.* **2006**, *9*, 788–793. [CrossRef]

59.	Chen, C.; Bai, H.; Chang, S.M.; Chang, C.; Den, W. Preparation of N-doped TiO$_2$ photocatalyst by atmospheric pressure plasma process for VOCs decomposition under UV and visible light sources. *J. Nanopart. Res.* **2007**, *9*, 365–375. [CrossRef]

60.	Panepinto, A.; Cossement, D.; Snyders, R. Experimental and theoretical study of the synthesis of N-doped TiO$_2$ by N ion implantation of TiO$_2$ thin films. *Appl. Surf. Sci.* **2021**, *541*, 148493. [CrossRef]

61.	Borras, A.; Lopez, C.; Rico, V.; Gracia, F.; Gonzalez-Elipe, A.R.; Richter, E.; Battiston, G.; Gerbasi, R.; McSporran, N.; Sauthier, G.; et al. Effect of visible and UV illumination on the water contact angle of TiO$_2$ thin films with incorporated nitrogen. *J. Phys. Chem. C* **2007**, *111*, 1801–1808. [CrossRef]

62.	Ghicov, A.; Macak, J.M.; Tsuchiya, H.; Kunze, J.; Haeublein, V.; Frey, L.; Schmuki, P. Ion Implantation and Annealing for an Efficient N-Doping of TiO$_2$ Nanotubes. *Nano Lett.* **2006**, *6*, 1080–1082. [CrossRef]

63.	Khan, T.T.; Bari, G.A.K.M.R.; Kang, H.-J.; Lee, T.-G.; Park, J.-W.; Hwang, H.J.; Hossain, S.M.; Mun, J.S.; Suzuki, N.; Fujishima, A.; et al. Synthesis of N-Doped TiO$_2$ for Efficient Photocatalytic Degradation of Atmospheric NOx. *Catalysts* **2021**, *11*, 109. [CrossRef]

64.	Ji, L.; Zhou, S.; Liu, X.; Gong, M.; Xu, T. Synthesis of carbon- and nitrogen-doped TiO$_2$/carbon composite fibers by a surface-hydrolyzed PAN fiber and their photocatalytic property. *J. Mater. Sci.* **2020**, *55*, 2471–2481. [CrossRef]

65.	Japa, M.; Tantraviwat, D.; Phasayavan, W.; Nattestad, A.; Chen, J.; Inceesungvorn, B. Simple preparation of nitrogen-doped TiO$_2$ and its performance in selective oxidation of benzyl alcohol and benzylamine under visible light. *Colloids Surf. A Physicochem. Eng. Asp.* **2020**, *610*, 125743. [CrossRef]

66.	Le, P.; Hieu, L.; Lam, T.N.; Hang, N.; Truong, N.; Tuyen, L.; Phong, P.T.; Leu, J. Enhanced Photocatalytic Performance of Nitrogen-Doped TiO$_2$ Nanotube Arrays Using a Simple Annealing Process. *Micromachines* **2018**, *9*, 618. [CrossRef]

67.	Mor, G.K.; Varghese, O.K.; Paulose, M.; Shankar, K.; Grimes, C.A. A review on highly ordered, vertically oriented TiO$_2$ nanotube arrays: Fabrication, material properties, and solar energy applications. *Sol. Energy Mater. Sol. Cells* **2006**, *90*, 2011–2075. [CrossRef]

68.	Wang, D.; Yu, B.; Wang, C.; Zhou, F.; Liu, W. A novel protocol toward perfect alignment of anodized TiO$_2$ nanotubes. *Adv. Mater.* **2009**, *21*, 1964–1967. [CrossRef]

69.	Pishkar, N.; Ghoranneviss, M.; Ghorannevis, Z.; Akbari, H. Study of the highly ordered TiO$_2$ nanotubes physical properties prepared with two-step anodization. *Results Phys.* **2018**, *9*, 1246–1249. [CrossRef]

70.	Mazierski, P.; Nischk, M.; Gołkowska, M.; Lisowski, W.; Gazda, M.; Winiarski, M.J.; Klimczuk, T.; Zaleska-Medynska, A. Photocatalytic activity of nitrogen doped TiO$_2$ nanotubes prepared by anodic oxidation: The effect of applied voltage, anodization time and amount of nitrogen dopant. *Appl. Catal. B Environ.* **2016**, *196*, 77–88. [CrossRef]

71.	Lai, Y.-K.; Huang, J.-Y.; Zhang, H.-F.; Subramaniam, V.-P.; Tang, Y.-X.; Gong, D.-G.; Sundar, L.; Sun, L.; Chen, Z.; Lin, C.-J. Nitrogen-doped TiO$_2$ nanotube array films with enhanced photocatalytic activity under various light sources. *J. Hazard. Mater.* **2010**, *184*, 855–863. [CrossRef]

72.	Wan, L.; Li, J.F.; Feng, J.Y.; Sun, W.; Mao, Z.Q. Improved optical response and photocatalysis for N-doped titanium oxide (TiO$_2$) films prepared by oxidation of TiN. *Appl. Surf. Sci.* **2007**, *253*, 4764–4767. [CrossRef]

73.	Liu, G.; Yang, H.G.; Wang, X.; Cheng, L.; Pan, J.; Lu, G.Q.M.; Cheng, H.-M. Visible light responsive nitrogen doped anatase TiO$_2$ sheets with dominant {001} facets derived from TiN. *J. Am. Chem. Soc.* **2009**, *131*, 12868–12869. [CrossRef]

74.	Cooper, E.; Andrews, C.; Wheatley, P.S.; Webb, P.B.; Wormald, P.; Morris, R.E. Ionic liquids and eutectic mixtures as solvent and template in synthesis of zeolite analogues. *Nature* **2004**, *430*, 1012–1016. [CrossRef] [PubMed]

75.	Pipi, A.; Byzynski, G.; Ruotolo, L. Photocatalytic activity and RNO dye degradation of nitrogen-doped TiO$_2$ prepared by ionothermal synthesis. *Mater. Res.* **2017**, *20*, 628–638. [CrossRef]

76.	Pratsinis, S.E. Flame aerosol synthesis of ceramic powders. *Prog. Energy Combust.* **1998**, *24*, 197–219. [CrossRef]

77.	Madler, L.; Kammler, H.K.; Mueller, R.; Pratsinis, S.E. Controlled synthesis of nanostructured particles by flame spray pyrolysis. *Aerosol Sci.* **2002**, *33*, 369–389. [CrossRef]

78.	Boningari, T.; Inturi, S.N.R.; Suidan, M.; Smirniotis, P.G. Novel one-step synthesis of nitrogen-doped TiO$_2$ by flame aerosol technique for visible-light photocatalysis: Effect of synthesis parameters and secondary nitrogen (N) source. *Chem. Eng. J.* **2018**, *350*, 324–334. [CrossRef]

79.	Kim, T.H.; Go, G.-M.; Cho, H.-B.; Song, Y.; Lee, C.-G.; Choa, Y.-H. A Novel Synthetic Method for N Doped TiO$_2$ Nanoparticles Through Plasma-Assisted Electrolysis and Photocatalytic Activity in the Visible Region. *Front. Chem.* **2018**, *6*, 458. [CrossRef]

80.	Nasirian, M.; Mehrvar, M. Photocatalytic degradation of aqueous Methyl Orange using nitrogen-doped TiO$_2$ photocatalyst prepared by novel method of ultraviolet-assisted thermal synthesis. *J. Environ. Sci.* **2018**, *66*, 81–93. [CrossRef]

81.	Yin, S.; Liu, B.; Sato, T. Microwave-Assisted Hydrothermal Synthesis of Nitrogen-Doped Titania Nanoparticles. *Funct. Mater. Lett.* **2008**, *1*, 173–176. [CrossRef]

82. Peng, Y.P.; Lo, S.L.; Ou, H.H.; Lai, S.W. Microwave-assisted hydrothermal synthesis of N-doped titanate nanotubes for visible-light-responsive photocatalysis. *J. Hazard. Mater.* **2010**, *183*, 754–758. [CrossRef]

83. Peng, F.; Cai, L.; Yu, H.; Wang, H.; Yang, J. Synthesis and characterization of substitutional and interstitial nitrogen-doped titanium dioxides with visible light photocatalytic activity. *J. Solid State Chem.* **2008**, *181*, 130–136. [CrossRef]

84. Irie, H.; Watanabe, Y.; Hashimoto, K. Nitrogen-Concentration Dependence on Photocatalytic Activity of $TiO_{2-x}N_x$ Powders. *J. Phys. Chem. B* **2003**, *107*, 5483–5486. [CrossRef]

85. Chen, X.; Burda, C. Photoelectron Spectroscopic Investigation of Nitrogen-Doped Titania Nanoparticles. *J. Phys. Chem. B* **2004**, *108*, 15446–15449. [CrossRef]

86. Sathish, M.; Viswanathan, B.; Viswanath, R.P.; Gopinath, C.S. Synthesis, Characterization, Electronic Structure, and Photocatalytic Activity of Nitrogen-Doped TiO_2 Nanocatalyst. *Chem. Mater.* **2005**, *17*, 6349–6353. [CrossRef]

87. Lee, H.U.; Lee, Y.C.; Lee, S.C.; Park, S.Y.; Son, B.; Lee, J.W.; Lim, C.H.; Choi, C.J.; Choi, M.H.; Lee, S.Y.; et al. Visible-light-responsive bicrystalline (anatase/brookite) nanoporous nitrogen-doped TiO_2 photocatalysts by plasma treatment. *Chem. Eng. J.* **2014**, *254*, 268–275. [CrossRef]

88. Cong, Y.; Zhang, J.; Chen, F.; Anpo, M. Synthesis and Characterization of Nitrogen-Doped TiO_2 Nanophotocatalyst with High Visible Light Activity. *J. Phys. Chem. C* **2007**, *111*, 6976–6982. [CrossRef]

89. Hu, Y.; Liu, H.; Kong, X.; Guo, X. Effect of calcination on the visible light photocatalytic activity of N-doped TiO_2 prepared by the sol-gel method. *J. Nanosci. Nanotechnol.* **2014**, *14*, 3532–3537. [CrossRef]

90. Suwannaruang, T.; Kidkhunthod, P.; Chanlek, N.; Soontaranon, S.; Wantala, K. High anatase purity of nitrogen-doped TiO_2 nanorice particles for the photocatalytic treatment activity of pharmaceutical wastewater. *Appl. Surf. Sci.* **2019**, *478*, 1–14. [CrossRef]

91. Mirzaei, A.; Eddah, M.; Roualdes, S.; Ma, D.; Chaker, M. Multiple-homojunction gradient nitrogen doped TiO_2 for photocatalytic degradation of sulfamethoxazole, degradation mechanism, and toxicity assessment. *Chem. Eng. J.* **2021**, *422*, 130507. [CrossRef]

92. Rani, A.; Dhiman, R.L.; Singh, V.; Kumar, S.; Kumar, S. Photocatalytic study of Ni-N-codoped TiO_2 nanoparticles under visible light irradiation. *Nano Express* **2021**, *2*, 030002. [CrossRef]

93. Alotaibi, A.M.; Promdet, P.; Hwang, G.B.; Li, J.; Nair, S.P.; Sathasivam, S.; Kafizas, A.; Carmalt, C.J.; Parkin, I.P. Zn and N Codoped TiO_2 Thin Films: Photocatalytic and Bactericidal Activity. *ACS Appl. Mater. Interfaces* **2021**, *13*, 10480–10489. [CrossRef]

94. Selcuk, M.Z.; Boroglu, M.S.; Boz, I. Hydrogen production by photocatalytic water-splitting using nitrogen and metal co-doped TiO_2 powder photocatalyst. *Reac. Kinet. Mech. Catal.* **2012**, *106*, 313–324. [CrossRef]

95. Lin, H.; Shih, C. Efficient one-pot microwave-assisted hydrothermal synthesis of M (M=Cr, Ni, Cu, Nb) and nitrogen co-doped TiO_2 for hydrogen production by photocatalytic water splitting. *J. Mol. Catal. A Chem.* **2016**, *411*, 128–137. [CrossRef]

96. Abdelraheem, W.H.M.; Patil, M.K.; Nadagouda, M.N.; Dionysiou, D.D. Hydrothermal synthesis of photoactive nitrogen- and boron- codoped TiO_2 nanoparticles for the treatment of bisphenol A in wastewater: Synthesis, photocatalytic activity, degradation byproducts and reaction pathways. *Appl. Catal. B Environ.* **2019**, *241*, 598–611. [CrossRef]

97. Abdelraheem, W.H.M.; Nadagouda, M.N.; Dionysiou, D.D. Solar light-assisted remediation of domestic wastewater by NB-TiO_2 nanoparticles for potable reuse. *Appl. Catal. B Environ.* **2020**, *269*, 118807. [CrossRef]

98. Cong, Y.; Zhang, J.; Chen, F.; Anpo, M.; He, D. Preparation, Photocatalytic Activity, and Mechanism of Nano-TiO_2 Co-Doped with Nitrogen and Iron (III). *J. Phys. Chem. C* **2007**, *111*, 10618–10623. [CrossRef]

99. Chen, D.; Jiang, Z.; Geng, J.; Wang, Q.; Yang, D. Carbon and Nitrogen Co-doped TiO_2 with Enhanced Visible-Light Photocatalytic Activity. *Ind. Eng. Chem. Res.* **2007**, *46*, 2741–2746. [CrossRef]

100. Yu, T.; Tan, X.; Zhao, L.; Yin, Y.; Chen, P.; Wei, J. Characterization, activity and kinetics of a visible light driven photocatalyst: Cerium and nitrogen co-doped TiO_2 nanoparticles. *Chem. Eng. J.* **2010**, *157*, 86–92. [CrossRef]

101. Thind, S.S.; Wu, G.; Chen, A. Synthesis of mesoporous nitrogen–tungsten co-doped TiO_2 photocatalysts with high visible light activity. *Appl. Catal. B Environ.* **2012**, *111–112*, 38–45. [CrossRef]

102. Kuvarega, A.T.; Krause, R.W.M.; Mamba, B.B. Nitrogen/Palladium-Codoped TiO_2 for Efficient Visible Light Photocatalytic Dye Degradation. *J. Phys. Chem. C* **2011**, *115*, 22110–22120. [CrossRef]

103. Zhang, Y.; Zhang, J.; Zhu, Z.; Yan, N.; Liu, Q. Preparation and properties of sliver and nitrogen co-doped TiO_2 photocatalyst. *Mater. Res. Bull.* **2013**, *48*, 4872–4876. [CrossRef]

104. Jaiswal, R.; Bharambe, J.; Patel, N.; Dashora, A.; Kothari, D.C.; Miotello, A. Copper and Nitrogen co-doped TiO_2 photocatalyst with enhanced optical absorption and catalytic activity. *Appl. Catal. B Environ.* **2015**, *168–169*, 333–341. [CrossRef]

105. El-Sheikh, S.M.; Khedr, T.M.; Hakki, A.; Ismail, A.A.; Badawy, W.A.; Bahnemann, D.W. Visible light activated carbon and nitrogen co-doped mesoporous TiO_2 as efficient photocatalyst for degradation of ibuprofen. *Sep. Purif. Technol.* **2017**, *173*, 258–268. [CrossRef]

106. Rajoriya, S.; Bargole, S.; George, S.; Saharan, V.K.; Gogate, P.R.; Pandit, A.B. Synthesis and characterization of samarium and nitrogen doped TiO_2 photocatalysts for photo-degradation of 4-acetamidophenol in combination with hydrodynamic and acoustic cavitation. *Sep. Purif. Technol.* **2019**, *209*, 254–269. [CrossRef]

107. Sharotri, N.; Sharma, D.; Sud, D. Experimental and theoretical investigations of Mn-N-co-doped TiO_2 photocatalyst for visible light induced degradation of organic pollutants. *J. Mater. Res. Technol.* **2019**, *8*, 3995–4009. [CrossRef]

108. Park, I.-S.; Chung, K.-H.; Kim, S.-C.; Kim, S.-J.; Park, Y.-K.; Jung, S.-C. Photocatalytic degradation of 1,4-dioxane and hydrogen production using liquid phase plasma on N- and Ni- codoped TiO_2 photocatalyst. *Mater. Lett.* **2021**, *283*, 128751. [CrossRef]

109. Ohtani, B. Photocatalysis A to Z—What we know and what we do not know in a scientific sense. *J. Photochem. Photobiol. C Photochem. Rev.* **2010**, *11*, 157–178. [CrossRef]

110. Natarajan, T.S.; Thampi, K.R.; Tayade, R.J. Visible light driven redox-mediator-free dual semiconductor photocatalytic systems for pollutant degradation and the ambiguity in applying Z-scheme concept. *Appl. Catal. B Environ.* **2018**, *227*, 296–311. [CrossRef]

111. Nakada, A.; Nishioka, S.; Vequizo, J.J.M.; Muraoka, K.; Kanazawa, T.; Yamakata, A.; Nozawa, S.; Kumagai, H.; Adachi, S.; Ishitani, O.; et al. Solar-driven Z-scheme water splitting using tantalum/nitrogen co-doped rutile titania nanorod as an oxygen evolution photocatalyst. *J. Mater. Chem. A* **2017**, *5*, 11710–11719. [CrossRef]

112. Miyoshi, A.; Kato, K.; Yokoi, T.; Wiesfeld, J.J.; Nakajima, K.; Yamakara, A.; Maeda, K. Nano vs. bulk rutile TiO_2:N,F in Z-scheme overall water splitting under visible light. *J. Mater. Chem. A* **2020**, *8*, 11996–12002. [CrossRef]

113. Burda, C.; Lou, Y.; Chen, X.; Samia, A.C.S.; Stout, J.; Gole, J.L. Enhanced Nitrogen Doping in TiO_2 Nanoparticles. *Nano Lett.* **2003**, *3*, 1049–1051. [CrossRef]

114. Nosaka, Y.; Matsushita, M.; Nishino, J.; Nosaka, A.Y. Nitrogen-doped titanium dioxide photocatalysts for visible response prepared by using organic compounds. *Sci. Technol. Adv. Mater.* **2005**, *6*, 143–148. [CrossRef]

115. Kalantari, K.; Kalbasi, M.; Sohrabi, M.; Royaee, S.J. Synthesis and characterization of N-doped TiO_2 nanoparticles and their application in photocatalytic oxidation of dibenzothiophene under visible light. *Ceram. Int.* **2016**, *42*, 14834–14842. [CrossRef]

116. RamezaniSani, S.; Rajabi, M.; Mohseni, F. Influence of nitrogen doping on visible light photocatalytic activity of TiO_2 nanowires with anatase-rutile junction. *Chem. Phys. Lett.* **2020**, *744*, 137217. [CrossRef]

117. Bakre, P.V.; Tilve, S.G.; Shirsat, R.N. Influence of N sources on the photocatalytic activity of N-doped TiO_2. *Arab. J. Chem.* **2020**, *13*, 7637–7651. [CrossRef]

118. Huang, J.; Dou, L.; Li, J.; Zhong, J.; Li, M.; Wang, T. Excellent visible light responsive photocatalytic behavior of N-doped TiO_2 toward decontamination of organic pollutants. *J. Hazard. Mater.* **2021**, *403*, 123857. [CrossRef]

119. Zeng, X.; Sun, X.; Wang, Y. Photocatalytic degradation of flumequine by N-doped TiO_2 catalysts under simulated sunlight. *Environ. Eng. Res.* **2021**, *26*, 200524. [CrossRef]

120. Tryba, B.; Wozniak, M.; Zolnierkiewicz, G.; Guskos, N.; Morawski, A.; Colbeau-Justin, C.; Wrobel, R.; Nitta, A.; Ohtani, B. Influence of an Electronic Structure of N-TiO_2 on Its Photocatalytic Activity towards Decomposition of Acetaldehyde under UV and Fluorescent Lamps Irradiation. *Catalysts* **2018**, *8*, 85. [CrossRef]

121. Li, D.; Haneda, H.; Hishita, S.; Ohashi, N. Visible-light-driven nitrogen-doped TiO_2 photocatalysts: Effect of nitrogen precursors on their photocatalysis for decomposition of gas-phase organic pollutants. *Mater. Sci. Eng. B* **2005**, *117*, 67–75. [CrossRef]

122. Aoki, K.; Morikawa, T.; Ohwaki, T.; Taga, Y. Photocatalytic Degradation of Formaldehyde and Toluene Mixtures in Air with a Nitrogen-doped TiO_2 Photocatalyst. *Chem. Lett.* **2006**, *35*, 616–617. [CrossRef]

123. Jo, W.-K.; Kim, J.-T. Application of visible-light photocatalysis with nitrogen-doped or unmodified titanium dioxide for control of indoor-level volatile organic compounds. *J. Hazard. Mater.* **2009**, *164*, 360–366. [CrossRef]

124. He, F.; Ma, F.; Li, T.; Li, G. Solvothermal synthesis of N-doped TiO_2 nanoparticles using different nitrogen sources, and their photocatalytic activity for degradation of benzene. *Chin. J. Catal.* **2013**, *34*, 2263–2270. [CrossRef]

125. Priya, V.S.; Philip, L. Photocatalytic Degradation of Aqueous VOCs Using N Doped TiO_2: Comparison of Photocatalytic Degradation under Visible and Sunlight Irradiation. *Int. J. Environ. Sci. Dev.* **2015**, *6*, 286–291. [CrossRef]

126. Zhao, C.; Wang, Z.; Chen, X.; Chu, H.; Fu, H.; Wang, C.-C. Robust photocatalytic benzene degradation using mesoporous disk-like N-TiO_2 derived from MIL-125(Ti). *Chin. J. Catal.* **2020**, *41*, 1186–1197. [CrossRef]

127. Suda, Y.; Kawasaki, H.; Ueda, T.; Ohshima, T. Preparation of high quality nitrogen doped TiO_2 thin film as a photocatalyst using a pulsed laser deposition method. *Thin Solid Film.* **2004**, *453–454*, 162–166. [CrossRef]

128. Joung, S.-K.; Amemiya, T.; Murabayashi, M.; Itoh, K. Relation between photocatalytic activity and preparation conditions for nitrogen-doped visible light-driven TiO_2 photocatalysts. *Appl. Catal. A Gen.* **2006**, *312*, 20–26. [CrossRef]

129. Fang, J.; Wang, F.; Qian, K.; Bao, H.; Jiang, Z.; Huang, W. Bifunctional N-Doped Mesoporous TiO_2 Photocatalysts. *J. Phys. Chem. C* **2008**, *112*, 18150–18156. [CrossRef]

130. Xing, M.; Zhang, J.; Chen, F. New approaches to prepare nitrogen-doped TiO_2 photocatalysts and study on their photocatalytic activities in visible light. *Appl. Catal. B Environ.* **2009**, *89*, 563–569. [CrossRef]

131. Tang, Y.C.; Huang, X.H.; Yu, H.Q.; Tang, L.H. Nitrogen-Doped Photocatalyst Prepared by Mechanochemical Method: Doping Mechanisms and Visible Photoactivity of Pollutant Degradation. *Int. J. Photoenergy* **2011**, *2012*, 960726.

132. Powell, M.J.; Dunnill, C.W.; Parkin, I.P. N-doped TiO_2 visible light photocatalyst films via a sol–gel route using TMEDA as the nitrogen source. *J. Photochem. Photobiol. A Chem.* **2014**, *281*, 27–34. [CrossRef]

133. Vaiano, V.; Sacco, O.; Sannino, D.; Ciambelli, P. Nanostructured N-doped TiO_2 coated on glass spheres for the photocatalytic removal of organic dyes under UV or visible light irradiation. *Appl. Catal. B Environ.* **2015**, *170–171*, 153–161. [CrossRef]

134. Huang, W.C.; Ting, J.M. Novel nitrogen-doped anatase TiO_2 mesoporous bead photocatalysts for enhanced visible light response. *Ceram. Int.* **2017**, *43*, 9992–9997. [CrossRef]

135. Calisir, M.D.; Gungor, M.; Demir, A.; Kilic, A.; Khan, M.M. Nitrogen-doped TiO_2 fibers for visible-light-induced photocatalytic activities. *Ceram. Int.* **2020**, *46*, 16743–16753. [CrossRef]

136. Divyasri, Y.V.; Reddy, N.L.; Lee, K.; Sakar, M.; Rao, V.N.; Venkatramu, V.; Shankar, M.V.; Reddy, N.C.G. Optimization of N doping in TiO_2 nanotubes for the enhanced solar light mediated photocatalytic H_2 production and dye degradation. *Environ. Pollut.* **2021**, *269*, 116170. [CrossRef] [PubMed]

137. Jadhav, P.S.; Jadhav, T.; Bhosale, M.; Jadhav, C.H.; Pawar, V.C. Structural and optical properties of N-doped TiO$_2$ nanomaterials. *Mater. Today Proc.* **2021**, *43*, 2763–2767. [CrossRef]

138. Fiorenza, R.; Mauro, A.D.; Cantarella, M.; Gulino, A.; Spitaleri, L.; Privitera, V.; Impellizzeri, G. Molecularly imprinted N-doped TiO$_2$ photocatalysts for the selective degradation of o-phenylphenol fungicide from water. *Mater. Sci. Semicond. Process.* **2020**, *112*, 105019. [CrossRef]

139. Xu, G.; Zhang, Y.; Peng, D.; Sheng, D.; Di Ma, Y.T.; Zhang, Y. Nitrogen-doped mixed-phase TiO$_2$ with controllable phase junction as superior visible-light photocatalyst for selective oxidation of cyclohexane. *Appl. Surf. Sci.* **2021**, *536*, 147953. [CrossRef]

140. Tzeng, J.-H.; Weng, C.-H.; Yen, L.-T.; Gaybullaev, G.; Chang, C.-J.; de Luna, M.D.G.; Lin, Y.-T. Inactivation of pathogens by visible light photocatalysis with nitrogen-doped TiO$_2$ and tourmaline-nitrogen co-doped TiO$_2$. *Sep. Purif. Technol.* **2021**, *274*, 118979. [CrossRef]

141. Lu, G.; Wang, X.; Wang, Y.; Shi, G.; Xie, X.; Sun, J. Anti-oxidative microstructure design of ultra-stable N-TiO$_2$ composite for the gaseous photodegradation reactions. *Chem. Eng. J.* **2021**, *408*, 127257. [CrossRef]

142. Li, H.; Yin, S.; Wang, Y.; Sato, T. Persistent Fluorescence-Assisted TiO$_{2-x}$N$_y$-Based Photocatalyst for Gaseous Acetaldehyde Degradation. *Environ. Sci. Technol.* **2012**, *46*, 7741–7745. [CrossRef]

143. Chen, X.; Shen, S.; Guo, L.; Mao, S.S. Semiconductor-based Photocatalytic Hydrogen Generation. *Chem. Rev.* **2010**, *110*, 6503–6570. [CrossRef]

144. Samokhvalov, A. Hydrogen by photocatalysis with nitrogen codoped titanium dioxide. *Renew. Sustain. Energy Rev.* **2017**, *72*, 981–1000. [CrossRef]

145. Kumaravel, V.; Mathew, S.; Bartlett, J.; Pillai, S.C. Photocatalytic hydrogen production using metal doped TiO$_2$: A review of recent advances. *Appl. Catal. B Environ.* **2019**, *244*, 1021–1064. [CrossRef]

146. Do, H.H.; Nguyen, D.L.T.; Nguyen, X.C.; Le, T.-H.; Nguyen, T.P.; Trinh, Q.T.; Ahn, S.H.; Vo, D.-V.N.; Kim, S.Y.; Le, Q.V. Recent progress in TiO$_2$-based photocatalysts for hydrogen evolution reaction: A review. *Arab. J. Chem.* **2020**, *13*, 3653–3671. [CrossRef]

147. Rahman, M.Z.; Kibria, M.G.; Mullins, C.B. Metal-free photocatalysts for hydrogen evolution. *Chem. Soc. Rev.* **2020**, *49*, 1887–1931. [CrossRef]

148. Babu, V.J.; Kumar, M.K.; Nair, A.S.; Kheng, T.L.; Allakhverdiev, S.I.; Ramakrishna, S. Visible light photocatalytic water splitting for hydrogen production from N-TiO$_2$ rice grain shaped electrospun nanostructures. *Int. J. Hydrog. Energy* **2012**, *37*, 8897–8904. [CrossRef]

149. Zhang, X.; Song, P.; Cui, X. Nitrogen-doped TiO$_2$ Photocatalysts Synthesized from Titanium Nitride: Characterizations and Photocatalytic Hydrogen Evolution Performance. *J. Adv. Oxid. Technol.* **2013**, *16*, 131–136. [CrossRef]

150. Wang, C.; Hu, Q.-Q.; Huang, J.-Q.; Deng, Z.-H.; Shi, H.-L.; Wu, L.; Liu, Z.-G.; Cao, Y.-G. Effective water splitting using N-doped TiO$_2$ films: Role of preferred orientation on hydrogen production. *Int. J. Hydrog. Energy* **2014**, *39*, 1967–1971. [CrossRef]

151. Fakhouri, H.; Pulpytel, J.; Smith, W.; Zolfaghari, A.; Mortaheb, H.R.; Meshkini, F.; Jafari, R.; Sutter, E.; Arefi-Khonsari, F. Control of the visible and UV light water splitting and photocatalysis of nitrogen doped TiO$_2$ thin films deposited by reactive magnetron sputtering. *Appl. Catal. B Environ.* **2014**, *144*, 12–21. [CrossRef]

152. Sun, S.; Gao, P.; Yang, Y.; Yang, P.; Chen, Y.; Wang, Y. N-Doped TiO$_2$ Nanobelts with Coexposed (001) and (101) Facets and Their Highly Efficient Visible-Light-Driven Photocatalytic Hydrogen Production. *ACS Appl. Mater. Interfaces* **2016**, *8*, 18126–18131. [CrossRef]

153. Esmat, M.; El-Hosainy, H.; Tahawy, R.; Jevasuwan, W.; Tsunoji, N.; Fukata, N.; Ide, Y. Nitrogen doping-mediated oxygen vacancies enhancing co-catalyst-free solar photocatalytic H$_2$ production activity in anatase TiO$_2$ nanosheet assembly. *Appl. Catal. B Environ.* **2021**, *285*, 119755. [CrossRef]

154. Villa, K.; Black, A.; Domènech, X.; Peral, J. Nitrogen doped TiO$_2$ for hydrogen production under visible light irradiation. *Sol. Energy* **2012**, *86*, 558–566. [CrossRef]

155. Lin, H.; Shih, C. Efficient One-Pot Microwave-Assisted Hydrothermal Synthesis of Nitrogen-Doped TiO$_2$ for Hydrogen Production by Photocatalytic Water Splitting. *Catal. Surv. Asia* **2012**, *16*, 231–239. [CrossRef]

156. Wang, C.; Hu, Q.Q.; Huang, J.Q.; Wu, L.; Deng, Z.H.; Liu, Z.G.; Liu, Y.; Cao, Y.G. Efficient hydrogen production by photocatalytic water splitting using N-doped TiO$_2$ film. *Appl. Surf. Sci.* **2013**, *283*, 188–192. [CrossRef]

157. Preethi, L.K.; Antony, R.P.; Mathews, T.; Loo, S.C.J.; Wong, L.H.; Dash, S.; Tyagi, A.K. Nitrogen doped anatase-rutile heterostructured nanotubes for enhanced photocatalytic hydrogen production: Promising structure for sustainable fuel production. *Int. J. Hydrog. Energy* **2016**, *41*, 5865–5877. [CrossRef]

158. Reddy, P.A.K.; Reddy, P.V.L.; Kim, K.H.; Kumar, M.K.; Manvitha, C.; Shim, J.J. Novel approach for the synthesis of nitrogen-doped titania with variable phase composition and enhanced production of hydrogen under solar irradiation. *J. Ind. Eng. Chem.* **2017**, *53*, 253–260. [CrossRef]

159. Liu, S.H.; Tang, W.T.; Lin, W.X. Self-assembled ionic liquid synthesis of nitrogen-doped mesoporous TiO$_2$ for visible-light-responsive hydrogen production. *Int. J. Hydrog. Energy* **2017**, *42*, 24006–24013. [CrossRef]

160. Xu, X.L.; Song, W. Enhanced H$_2$ production activity under solar irradiation over N-doped TiO$_2$ prepared using pyridine as a precursor: A typical sample of N-doped TiO$_2$ series. *Mater. Technol.* **2017**, *32*, 52–63. [CrossRef]

161. Zangeneh, H.; Farhadiana, M.; Zinatizadeh, A.A. A reusable visible driven N and C–N doped TiO$_2$ magnetic nanocomposites for photodegradation of direct red 16 azo dye in water and wastewater. *Environ. Technol.* **2020**, 1–16. [CrossRef]